

FEATURE ARTICLE

Biomolecular Electronics: Protein-Based Associative Processors and Volumetric Memories

Robert R. Birge,* Nathan B. Gillespie, Enrique W. Izaguirre, Anakarin Kusnetzow, Albert F. Lawrence, Deepak Singh, Q. Wang Song, Edward Schmidt, Jeffrey A. Stuart, Sukeerthi Seetharaman, and Kevin J. Wise

W. M. Keck Center for Molecular Electronics and Department of Chemistry, Syracuse University, Syracuse, New York 13244

Received: June 9, 1999; In Final Form: September 3, 1999

The promise of new architectures and more cost-effective miniaturization has prompted interest in molecular and biomolecular electronics. Bioelectronics offers valuable near-term potential, because evolution and natural selection have optimized many biological molecules to perform tasks that are required for device applications. The light-transducing protein bacteriorhodopsin provides not only an efficient photonic material, but also a versatile template for device creation and optimization via both chemical modification and genetic engineering. We examine here the use of this protein as the active component in holographic associative memories as well as branched-photocycle three-dimensional optical memories. The associative memory is based on a Fourier transform optical loop and utilizes the real-time holographic properties of the protein thin films. The three-dimensional memory utilizes an unusual branching reaction that creates a long-lived photoproduct. By using a sequential multiphoton process, parallel write, read, and erase processes can be carried out without disturbing data outside of the doubly irradiated volume elements. The methods and procedures of prototyping these bioelectronic devices are discussed. We also examine current efforts to optimize the protein memory medium by using chemical and genetic methods.

1. Introduction

Molecular electronics is broadly defined as the encoding, manipulation, and retrieval of information at a molecular or macromolecular level. This approach contrasts with current techniques, in which these functions are accomplished via lithographic manipulation of bulk materials to generate integrated circuits. A key advantage of the molecular approach is the ability to design and fabricate devices from the “bottom-up”, on an atom-by-atom or residue-by-residue basis. It is unlikely that lithography will ever provide the level of control available through organic synthesis or genetic engineering. Two commonly stated rationales for exploring molecular electronics are the potential of significant decreases in both device feature sizes and gate propagation delays. A molecular computer could, in principle, be 2–3 orders of magnitude smaller and faster than a present day semiconductor computer composed of a comparable number of logic gates. However, extrapolation of Moore’s law¹ predicts that semiconductor feature sizes will approach the molecular domain around 2030.² There are two possible scenarios. The first is that Moore’s law will remain valid until 2030 and that lithographic techniques will evolve to create nanoscale devices with properties much like those currently envisioned for molecular devices. The second scenario is that

semiconductor evolution will “hit a wall” for economic reasons, and computer technologists will redirect their efforts toward the exploration of new architectures rather than smaller feature sizes.³ In either case, molecular electronics will play an ever increasing role in the development of computer devices. While size and speed are adequate reasons for exploring molecular electronics, we suggest that it is the opportunity to create new hybrid architectures that provides molecular electronics with the more significant comparative advantage. Liquid crystal displays (LCDs) represent one well-known commercial success of molecular electronics. While demonstrating the potential, LCDs should be viewed as a representative first success of a new and largely unexplored hybrid molecular and semiconductor technology.

Bioelectronics is a subfield of molecular electronics that investigates the use of native as well as modified biological molecules (chromophores, proteins, etc.) in electronic or photonic devices. Because evolution has often solved problems of a nature similar to those that must be solved in harnessing organic compounds and because self-assembly and genetic engineering provide sophisticated control and manipulation of large molecules or ensembles, bioelectronics has shown considerable promise. Much of the current research effort in bioelectronics is directed toward self-assembled monolayers and thin films, biosensors, and protein-based photonic devices.

* Direct correspondence to this author (e-mail: rbirge@syr.edu).

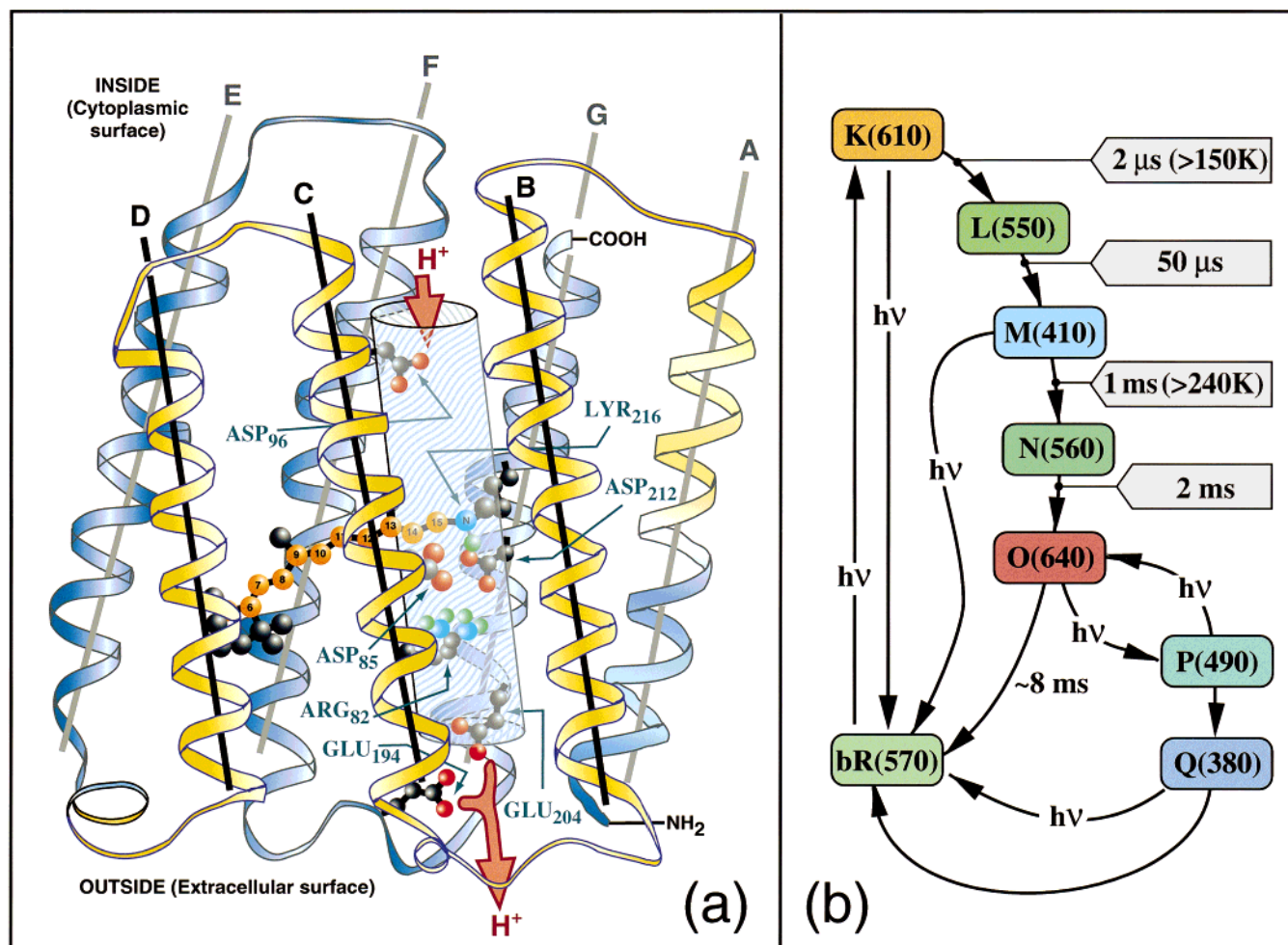


Figure 1. Simplified structure of the protein (a, backbone structure from ref 11) and the key intermediates in the primary and branched photocycle (b) of bacteriorhodopsin. Wavelength maxima (in parentheses, nm), lifetimes, and temperatures apply to the wild-type only and are approximate.

Although a number of proteins have been explored for device applications,^{4–8} bacteriorhodopsin has received the most attention. Russian scientists, under the leadership of the late Yuri Ovchinnikov, were the first to recognize and explore the potential of bacteriorhodopsin. Ovchinnikov was not only a highly respected molecular biologist and director of the Shemyakin Institute but also a forceful advocate of bioelectronics within the decision-making apparatus of the former Soviet Union. He proposed that Soviet science could leapfrog the West in computer technology by exploring bioelectronics and garnered significant funding to explore this possibility under what became known as “Project Rhodopsin”. Many of the applications were military and the details are obscure (i.e., remain classified). Nevertheless, the photochromic and holographic properties of this protein were published and stimulated an international research effort that continues today. One of the best-known accomplishments of this project was the development of *Biochrome*, a real-time photochromic and holographic film based on chemically modified polymer films containing bacteriorhodopsin.^{9,10} The principal investigator of this project, Nikolai Vsevolodov, has since moved to the U.S. and serves as the principal scientist of Starzent, a small start-up company that seeks to manufacture high-density holographic memories. Vsevolodov’s recent book provides an excellent introduction to the field of protein-based devices.⁴

Bacteriorhodopsin (BR) is grown in the purple membrane of a salt marsh bacterium called *Halobacterium salinarium* (aka

Halobacterium halobium) (Figure 1).^{11–15} When we consider the nature of a salt marsh and the fact that this protein is designed for photosynthetic light energy transduction, we should not be surprised that a microorganism has created, albeit unwittingly, a material with comparative advantages in photonic devices. The protein must operate at high temperatures, under high light fluxes, for extended periods of time for the organism to survive. Furthermore, the protein must function under the chemical stress imposed by a pH gradient that the protein itself creates. What is surprising, however, is the broad range of applications for which this protein shows comparative advantage. These include random access thin film memories,^{16–18} neural-type logic gates,¹⁹ photon counters and photovoltaic converters,^{20–22} reversible holographic media,^{23,24} artificial retinas,^{25–27} picosecond photodetectors,^{28,29} spatial light modulators,^{7,30,31} associative memories,⁷ two-photon volumetric memories,^{30,32} holographic correlators,³³ nonlinear optical filters,³⁴ dynamic time-average interferometers,³⁵ optical limiters,³¹ pattern recognition systems,³⁶ real-time holographic imaging systems,³⁷ multilevel logic gates,³⁸ optical computing,³⁹ and branched-photocycle volumetric memories.^{40–43}

The goal of the present article is to explore the application of bacteriorhodopsin in two of the above-mentioned devices, a holographic associative memory that makes use of the real-time holographic capabilities of protein thin films, and a three-dimensional memory that makes use of an unusual branching reaction within the photocycle. The methods and procedures of

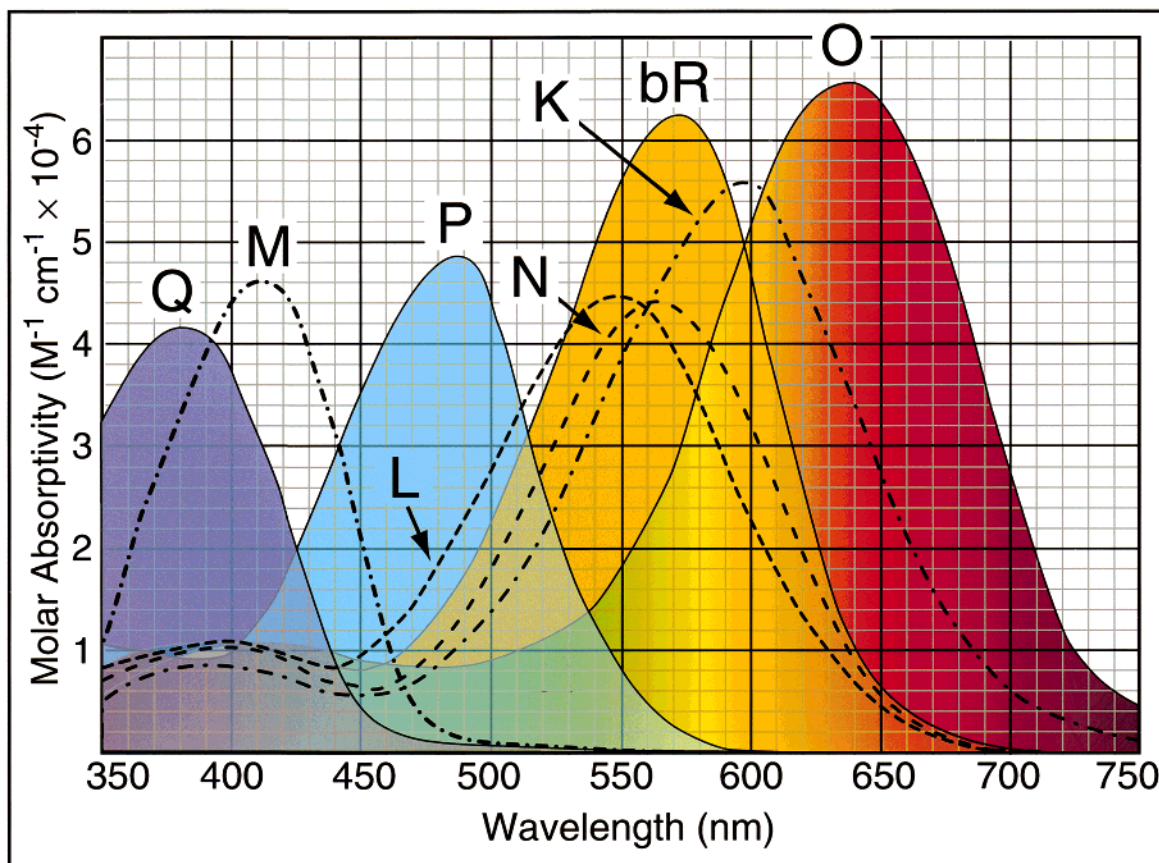


Figure 2. Ambient temperature absorption spectra of selected intermediates based on the studies of Varo and Lanyi (main photocycle from ref 47) and our studies (P and Q).

prototyping and reliability measurement will be presented with an emphasis on the three-dimensional memory, which is in the second generation of prototype development. While the native protein can be used in both devices, chemical or mutagenic modification improves performance. We therefore explore both approaches to materials optimization, as well as the principal reliability issues that remain to be solved.

2. Bacteriorhodopsin as a Photonic Material

Bacteriorhodopsin has seven trans-membrane α -helices that make up the protein's secondary structure (Figure 1). The production of the purple membrane allows the organism to switch to photosynthesis as a means of energy production, when dissolved oxygen concentrations drop below levels sufficient to sustain respirative oxidative phosphorylation. The light absorbing chromophore in the light-adapted form of the protein (bR_{LA} or simply bR) is all-trans retinal (polyene carbon atoms are colored orange in Figure 1a) covalently bound to Lys-216 via a protonated Schiff base linkage. The absorption of light by bR initiates a complex photochemical cycle of approximately 10 ms in duration, as shown in Figure 1b. The photocycle transports a proton from the intracellular to the extracellular side of the membrane. This light-induced proton pumping generates an electrochemical gradient that the bacterium uses to chemiosmotically synthesize ATP.

Photochemical stability is quantified as the number of times a photochromic material can be photoconverted between two species before 37% (1/e) of the irradiated ensemble denatures. This number is called the cyclicity, and it exceeds 10^6 for bacteriorhodopsin at ambient temperature.^{7,44} Few organic

photochromic materials approach this value, and those that have high cyclicities typically have low quantum efficiencies for photoconversion.^{45,46} The high cyclicity of bR is due to the protective features of the integral membrane protein that serves to isolate the chromophore from reactive oxygen, singlet oxygen, and free radicals. Thus, the common assumption that biological materials are too photolabile to be used in optoelectronic devices does not apply to bacteriorhodopsin.

The absorption spectra of the key photocycle intermediates⁴⁷ and branching photoproducts are shown in Figure 2. The absorption spectrum of each intermediate is due to changes in the geometry of the chromophore as well as changes in the binding site, and the detailed molecular origins remain to be determined. Even in the resting state, the electrostatic nature of the binding site has remained a subject of controversy (see discussion in ref 48). A majority of the evidence suggests that the counterion structure in the binding site generates a quadrupole with the chromophore and Arg-82 forming two positive charges separated by two negative residues, Asp-85 and Asp-212.^{48–50} Through genetic engineering and/or chemical modification, the dispersive and electrostatic properties of the binding site can be modified to yield analogue proteins with different spectroscopic and photochemical properties.^{7,36,44,51–57} The following sections examine selected photochemical processes and intermediates that are relevant to the present device applications.

2.1. The Excitation Process and the Primary Photochemical Event. The primary photochemical event of light-adapted bacteriorhodopsin involves two, subpicosecond processes. The first process is excitation of the chromophore to produce the Franck–Condon excited state. This nearly instantaneous event

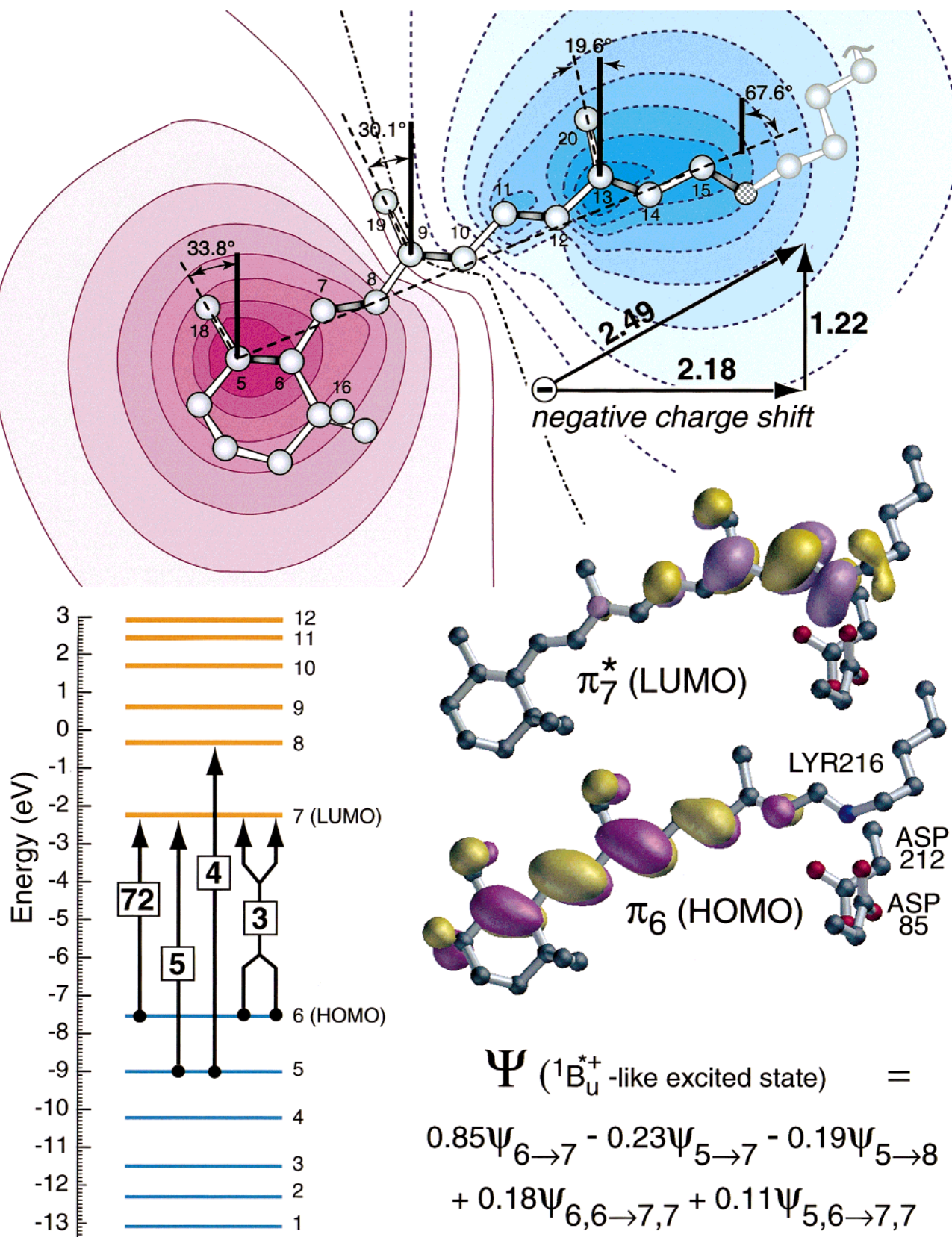


Figure 3. Excitation into the lowest-lying, strongly allowed excited state is well-described as a single electron (HOMO \rightarrow LUMO). The nearly barrier-less excited state potential surfaces for the all-trans to 13-cis photoisomerization (see Figure 4) are due to interaction between the increased charge density near the nitrogen atom and the nearby Asp-85 and Asp-212 negatively charged residues.

has a measurable photovoltaic consequence due to the large shift in electron density that accompanies electronic excitation of a long-chain, protonated Schiff-base polyene (Figure 3). The large shift in electron density is equivalent to moving an electron ~ 2.5

Å down the polyene chain toward the nitrogen atom, and this shift makes the $C_{14}C_{15}H=NH$ -Lys linkage more negative. The once favorable electrostatic interactions between the $C_{14}C_{15}H=NH$ -Lys and the two nearby negative Aspartic acid residues

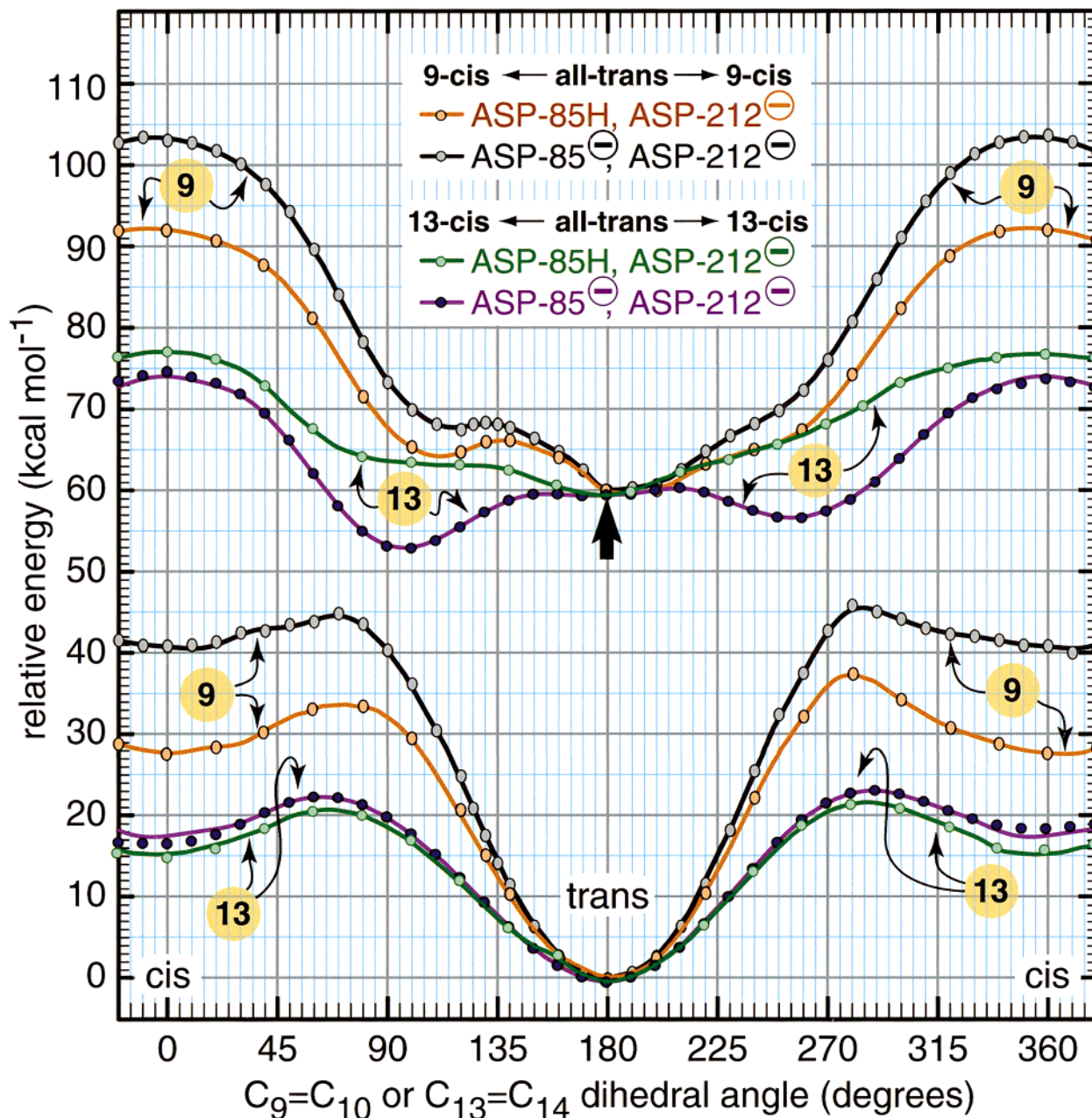


Figure 4. The ground and first excited singlet state potential energy surfaces for isomerization of the all-trans chromophore to form the 9-cis or 13-cis species are sensitive to the protonation state of the two nearby aspartic acid residues. Here we examine the influence of the protonation state of Asp-85. Adapted from ref 55.

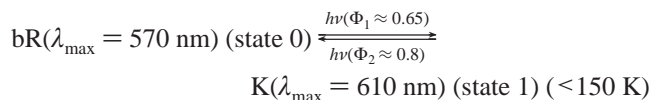
(Asp-85 and Asp-212) are now repulsive, and this interaction helps direct the photoisomerization about the 13-cis double bond to generate the primary photochemistry.⁷ This electrostatic interaction coupled with significant bond order reversal due to the excitation process (Figure 3) is sufficient to generate a nearly barrierless excited state potential surface for 13-trans to 13-cis photoisomerization (Figure 4). Thus, the barrier to isomerization in the ground state is altered dramatically in the excited state and yields what has been characterized as the biological equivalent of a high-electron mobility transistor.⁷ The photoisomerization is electrostatically selected, because the protonation of Asp-85 changes the excited-state surfaces dramatically and makes the formation of the 9-cis photoproduct competitive with the 13-cis photoproduct (see Figure 4 and discussion below). This possibility is exploited in the branched-photocycle volumetric memory (section 5).

The photoisomerization process also generates a photovoltaic signal due to the motion of the protonated Schiff base away from the negative counterions. However, relaxation of the chromophore and the protein following isomerization is complex, and deconvolution of the various components of the fast photovoltage is not yet possible. It is known that the primary photochemical event is a subpicosecond phenomenon^{58–60} and recent studies suggest a small barrier to isomerization.⁶¹ It is likely that the photovoltaic signal observed on the picosecond time scale from bacteriorhodopsin⁶² has contributions from both the excitation and photoisomerization process.

The primary photoproduct of bacteriorhodopsin is called J by many investigators, and K by others. Our early hypothesis that J is an inhomogeneous mixture of ground and excited-state species,⁶³ is consistent with some time-resolved fluorescence

studies⁶⁴ but inconsistent with other studies^{59–61} (see discussion in ref 12). A key observation is that J cannot be trapped at temperatures as low as 4 K. The current evidence suggests that J is vibrationally hot K. The K state is stable at temperatures below 150 K, and a binary photochemical system can be generated:^{56,65,66}

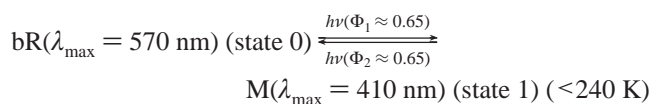
SCHEME 1



The interconversions share high quantum efficiencies, and cryogenic thin film disk memories have been made on the basis of this photoconversion.⁷ These memories are fast and efficient and may have application in those rare instances where liquid nitrogen cooling is available, and the storage of classified or proprietary information requires that the data be labile to prevent unauthorized access. The latter capability derives from the fact that all data stored in the K intermediate will be lost irretrievably upon warming the storage medium to ambient temperature.

2.2. The Metastable, Blue-Shifted M State. Most holographic applications of bacteriorhodopsin make use of the M state, and the photochemical process:^{56,67,68}

SCHEME 2



The relevance of this photoreaction derives from the significant blue shift of the M state relative to the resting state (bR). This spectroscopic change induces a large change in refractive index of the medium following photoconversion (Figure 5). At temperatures above 240 K, the M state decays thermally back to bR, as shown in Figure 1b. The intrinsic lifetime of the M state can be controlled by both chemical and genetic modifications to produce real-time holographic films with variable relaxation times. Invariably, one seeks to increase the lifetime of M, because the native protein has an M state lifetime of only a few milliseconds, which is too short for the majority of applications. Site-directed mutagenesis normally targets residues that participate in coupling the proton from the cytoplasmic surface to the Schiff base, and because the M → N transition involves reprotonation of the Schiff base, any interference in this process will stabilize the M state.^{53,69–72} The most commonly used mutation is D96N (Asp-96 → Asn-96), which generates an M state with a lifetime ranging from ~200 ms at pH 5 to ~20 s at pH 8, a range optimal for real-time holography.^{36,44} Chemicals can also be added to disrupt the reprotonation process, and many compounds were studied during the development of *Biochrome*.^{9,10} The best results have been obtained by adding polar or charged amines such as guanidine hydrochloride or diaminopropane (see section 3.5 below).⁷³ A more drastic approach is to replace the native all-trans retinal chromophore with a chromophore analogue.⁵¹ The incorporation of 4-keto retinal provides a dramatic increase in the M state lifetime, although the molecular mechanism is not well understood.^{57,74} A combination of the 4-keto chromophore with chemicals or double mutations [e.g., Thr-46 → Asn-46 + Asp-96 → Asn-96] yields correspondingly longer M state lifetimes that extend to many hours.

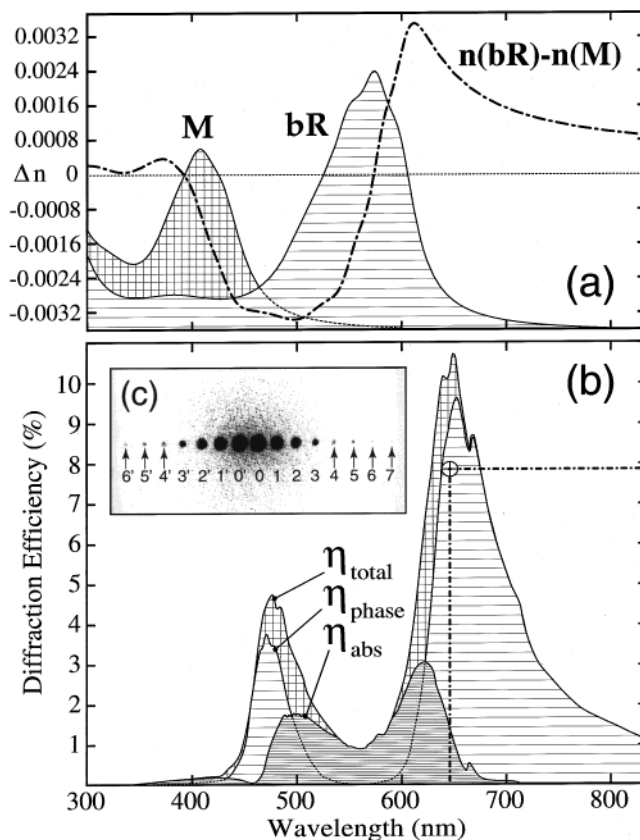


Figure 5. The change in refractive index associated with the bR → M photoreaction for a 30 μm film of bacteriorhodopsin with an optical density maximum of ~6 is shown as a function of wavelength in the upper panel. The refractive index change is calculated by using the Kramers–Kronig transformation assuming bR (100%) → M (100%) photoconversion. The absorption spectra of bR and M are shown for reference. The diffraction efficiency is shown in the lower panel and is calculated on the basis of the Kogelnik approximation. The dot at ~647 nm and ~8% diffraction efficiency is an experimental result for the film described above (after refs 32 and 104).

2.3. The Branched-Photocycle and the P and Q States.

Bacteriorhodopsin has a branching reaction from the main photocycle that appears to be of no relevance to the native organism but provides a means of generating a long-lived intermediate optimal for volumetric data storage (Figure 1b). The branching reaction in question involves the photoconversion of the O state to form a 9-cis species, which is called P (Figure 6). The 9-cis chromophore is unstable in the binding site due to steric interactions between the C9 and C13 methyl groups and nearby residues (see Figures 6b and 6c).⁵⁵ The instability is relieved via hydrolysis of the protonated Schiff base linkage by water to produce a free 9-cis retinal chromophore. Experimental and theoretical studies predict that the 9-cis chromophore remains contained within the protein interior. The resulting state is called Q, and while this state has been observed by many groups experimentally, it was not well understood until the elegant studies of Popp et al.⁷⁵ Because the formation of P (and ultimately Q) requires a sequential multiphoton process, these states are rarely observed and can be mistaken for denatured protein. A key indicator of the formation of P and/or Q is the ability to revert quantitatively the yellow material back to bR by using blue light. The lifetime of P is variable and depends on hydration, pH, and medium. The P state lasts for a few minutes in hydrated gels and for extended periods in dried poly(vinyl alcohol) thin films. (If one is designing a memory that is based on the storage of data in Q, it is best to design the memory

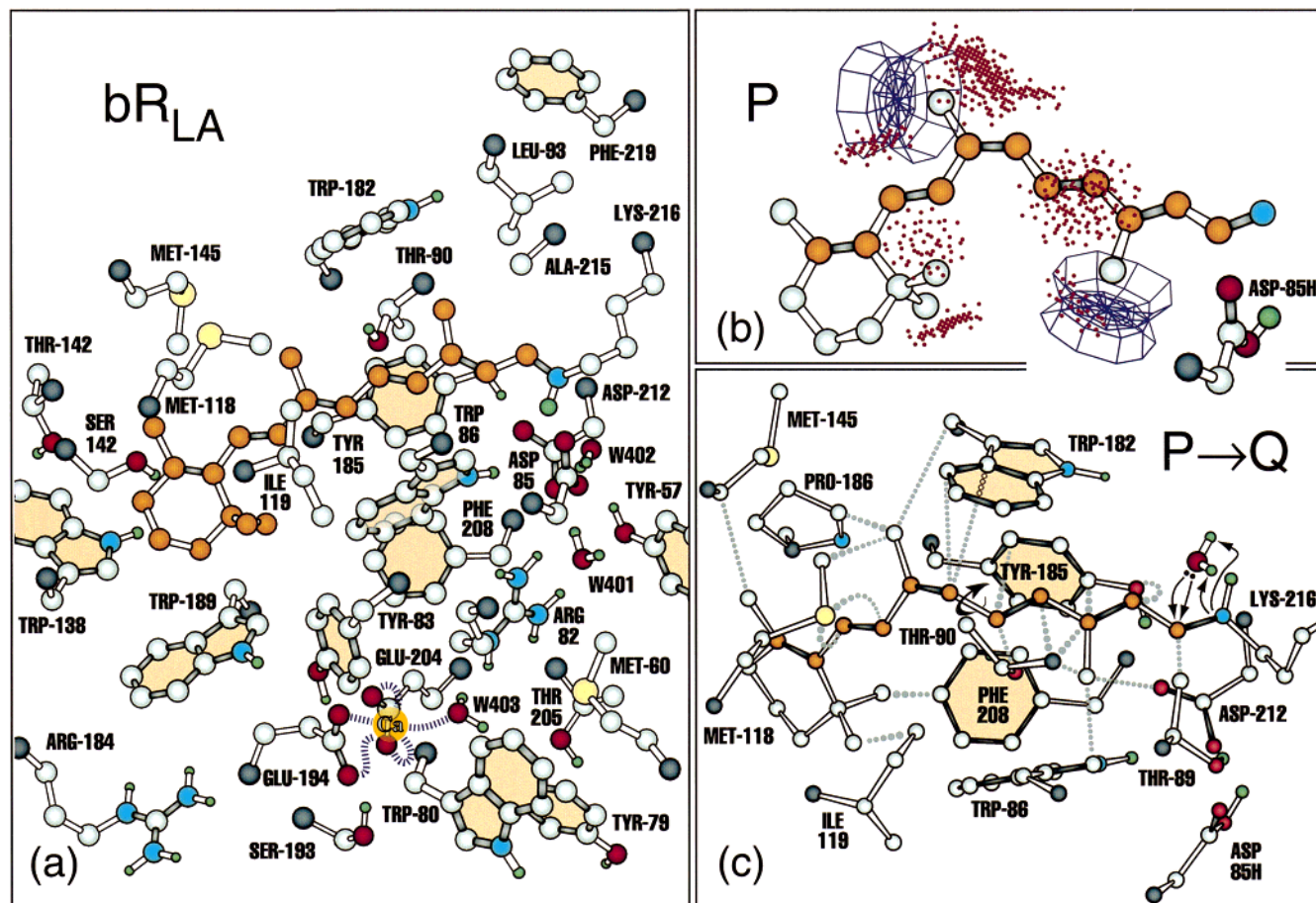


Figure 6. The nature of the bR binding site⁵⁰ is shown in (a). The formation of the 9-cis species within the binding site produces repulsion between the two chromophore methyl groups and the nearby protein residues as depicted in the energy (repulsion) map shown in (b). The key chromophore–protein residue interactions are shown in (c). These interactions destabilize the 9-cis chromophore and induce hydrolysis of the chromophore to form Q (9-cis retinal trapped within bacterio-opsin) (c). The barrier to isomerization of the 9-cis retinal chromophore to re-form the all-trans conformation is calculated to be 44.68 kcal mol⁻¹ within the protein matrix. Adapted from ref 55.

to treat both P and Q as the same bit state. This approach is used for the volumetric memory discussed below.) What makes the branching reaction so valuable for device applications is the long lifetime of the Q state, which is predicted to be 5–20 years. The calculated barrier for 9-cis → 9-trans thermal isomerization of the chromophore in the binding site is 45 kcal mol⁻¹, comparable to the activation energy for thermal denaturation of the protein.

A detailed molecular and quantum mechanical picture of the branching process is not available. Part of the problem is that we know relatively little about the nature of the binding site in the O state. The O state cannot be trapped, but spectroscopic studies indicate that the chromophore is all-trans and that Asp-85 is protonated in the O state. The potential energy surfaces presented in Figure 4 provide a perspective on the preferential formation of 13-cis photoproducts from bR but 9-cis photoproducts from O. This follows from the fact that the O state is similar to the blue membrane of bacteriorhodopsin, which is formed at low pH or upon deionization of the purple membrane. Indeed, the surfaces shown in Figure 4 and the binding site analysis of the P state in Figure 5 are actually based on simulations carried out on the blue membrane.⁵⁵

2.4. The Blue Membrane and Its SDM Variants. The above sections describe the key photochromic reactions relevant to most of the device applications of bacteriorhodopsin. We conclude this overview with a brief discussion of an alternative preparation of the protein that has received little attention but has significant potential. The “blue membrane” is a modified

form of the protein that is prepared by using low pH, rigorous removal of cations, or site-directed mutagenesis.^{55,76–79} The chemical or site-directed mutagenesis (SDM) variants share in common the protonation or neutral replacement of Asp-85 and a red shift of the absorption maximum of the resting state to 600 nm. Photoactivation of this species generates a long-lived 9-cis photoproduct that has a maximum at about 485 nm.^{55,77–79} Unfortunately, the quantum efficiencies of these phototransformations are relatively low (2×10^{-4} to 7×10^{-3}).^{55,80} A double mutant involving Asp-85 → Asn-85 and Asp-96 → Asn-96 provides a very successful, blue-membrane-like variant that is currently under study by a number of groups for long-term holographic data storage.^{78,79}

2.5. Nonlinear Spectroscopic Properties. Bacteriorhodopsin has a large two-photon absorptivity ($\delta = 290 \times 10^{-50}$ cm⁴ s molecules⁻¹ photon⁻¹) that permits the efficient activation of the primary event via long wavelength lasers.^{81,82} The protein also has large second- and third-order hyperpolarizabilities.^{83,84} The properties derive in large part from the large change in dipole moment, $\Delta\mu = 13.5 \pm 0.8$ D, that accompanies excitation into the lowest-lying strongly allowed “¹B_u^{*+}” state (see Figure 3).

3. Methods

We examine here the methods and procedures that are relevant to the preparation and manipulation of bacteriorhodopsin for device applications. The large range of methods available

for optimizing biological molecules represents a comparative advantage of bioelectronics. In addition to the methods described below, there are a number of research groups investigating the use of directed evolution, which may yield an exciting new group of bacteriorhodopsin variants with unusual and useful properties.

3.1. Preparation and Purification of Bacteriorhodopsin.

The goal of preparing bacteriorhodopsin for device applications is to achieve an adequate level of both purity and homogeneity while maximizing yield. Our methods are based on the standard methods^{85,86} with modifications that enhance homogeneity of the protein by using growth procedures that minimize the formation of nonmatured forms of the protein.^{87,88} A key feature of the revised preparative procedures is replacement of the sucrose density gradient with differential centrifugations. We have recently reviewed our methods of growing, isolating, and purifying bacteriorhodopsin for device applications, and we direct the reader to ref 88 for details.

When bacteriorhodopsin is isolated and purified via the above techniques, the resulting preparation is in the form of purple membrane patches, with diameters of approximately 500 nm, suspended in water. These patches are normally sonicated to smaller size (~100–180 nm) to reduce light scattering. The thermal stability of the protein derives in part from the maintenance of the purple membrane semicrystalline structure,^{89,90} and oversonication should be avoided.

3.2. Site-Directed Mutagenesis. Transformations of expression vectors into *Halobacterium salinarium* were conducted according to the protocol described by Ni et al.,⁹¹ which represents a modification of the original protocol of Cline and Doolittle.⁹² We used the expression vector pNovR, which contains the amino acid sequences encoding the bacteriorhodopsin gene product, upstream regulatory sequences, and Novobiocin resistance for selection. pNovR was transfected into *Halobacterium halobium* strain L33 lacking the ability to produce the bacteriorhodopsin protein. The L33 strain contains an insertional element “knock-out” of the bacteriorhodopsin gene and produces cells that appear white instead of purple (i.e., white membrane). Only reintroduction of an uninterrupted bacteriorhodopsin gene sequence (or a sequence modified at specific residues) can restore production of the protein. Both pNovR and L33 were kindly provided by Dr. Richard Needleman. Homologous recombination into *Halobium* is employed as described by Ferrando et al.⁹³

Mutations are constructed by using Stratagene’s Quick-Change site-directed mutagenesis kit. DNA primers were designed ranging from 30 to 35 base pairs in length with the mutation of interest centered between regions of homologous sequence. A silent restriction site was introduced in the primer sequence to monitor the introduction of the amino acid change. All sequences were verified by DNA sequencing to ensure the presence of one, and only one, amino acid substitution.

Mutagenesis and expression are also constructed in pMR4-Blue, provided by C. L. Winter and M. S. Braiman (unpublished), which was derived from pMR4 (M. Rudiger and D. Oesterhelt, unpublished). Like pNovR, pMR4-Blue contains Novobiocin resistance for selection of transformed plasmids in the native organism, as well as upstream regulatory sequences necessary for bacteriorhodopsin expression. Double mutations were constructed by using an expression vector containing a single mutation as a template in combination with mutagenic primers for the second amino acid to be altered. Similarly, triple mutations were constructed using an expression vector contain-

ing double mutations as a template and primers containing the third amino acid substitution.

Colonies are plated and grown in high salt media. Protein patches containing the mutant bacteriorhodopsin gene product were isolated and purified as described in section 3.1.

3.3. Random Mutagenesis. Two methods are used to generate random mutations, PCR (Polymerase Chain Reaction) mismatch and randomized expression using error prone competent cells. Both strategies introduce multiple, random mutations into the DNA sequence, but they yield slightly different results and offer comparative advantages and disadvantages. A key to using random mutagenesis to optimize materials is the ability to screen the mutants for the desired properties (see below).

PCR mismatch generates random amino acid substitutions in as many as 12 consecutive residues.⁹⁴ Primers composed of random nucleotides are used to generate multiple permutations in a given region. Because these sequences must be flanked by regions of homology for the primers to anneal properly, this technique is limited for random mutagenesis of up to 12 consecutive base pairs only. Once a successful mutation is located via SDM, PCR mismatch can be used to “fine tune” the protein to meet specific requirements (i.e., increased O state lifetime, increased O → P transition). By limiting modifications to the same local region, this technique can selectively enhance single mutations while leaving all other regions of the protein undisturbed. Another advantage of this technique is the compatibility of this technique with existing site-directed approaches; both were designed to work with the Stratagene Quick-Change mutagenesis systems in use in our lab.

Stratagene XL-I red competent cells are available from Stratagene and contain mutations that render the cells deficient in three of the primary DNA repair pathways in *E. coli*: *mutS*, *mutD*, and *mutT*.^{95,96} The use of this cell line makes the mutation rate approximately 5000-fold higher than that inherent in wild-type cell lines. The advantage of this approach is that as the cells grow they continue to introduce mutations in the DNA sequence. The disadvantage is that colonies will continue to mutate so that a single mutation with the desired properties can be lost via further, deleterious mutation(s). This process has a further disadvantage in that the number of mutations generated can quickly overwhelm ones ability to screen (see below).

Random mutant screening is carried out by using a modified light microscope that measures the photochemical properties of each individual colony in situ. The photocycle of the ensemble is excited by a 630 nm diode laser and the time-resolved spectroscopic properties are followed at four selected wavelengths by using a set of individual photomultipliers coupled to interchangeable interference filters. The output signals are collected by using a four-channel HP Infinium oscilloscope. The branching properties of the protein system can also be examined photochemically by using a Coherent Infinity XPO system, which generates 4 ns pulses from 430 to 700 nm to provide a second pump beam. In this fashion, random mutants with enhanced M, O, and Q states can be screened by using the same apparatus. The study of in situ colonies generates considerable noise, which precludes quantitative comparisons. Candidate colonies must be grown and the protein purified for quantitative comparison studies.

3.4. Chromophore Analogue Substitution. To introduce a new chromophore into the protein, the native retinal chromophore must first be removed. In the presence of hydroxylamine hydrochloride (Sigma H 9876), high pH (~8.5, TAPS Buffer, Sigma T 9659), and high illumination, the retinal

chromophore will undergo photochemical processes that generate bacterio-opsin and retinal (in the form of retinal oxime) embedded in the lipid membrane. The process of bleaching the protein takes 10–15 h at room temperature, and light above 500 nm should be used to avoid denaturation of the apoprotein. The extent of bleaching can be traced spectroscopically by observing the decrease in absorbance at 570 nm and the consequent increase in absorbance at 360 nm, due to the retinal oxime. After excess hydroxylamine hydrochloride has been removed and the apoprotein (apomembrane) is concentrated via centrifugation, a synthetically derived chromophore analogue can be added as a 2–4-fold molar excess in a minimum amount of 95% ethanol.⁹⁷ The reconstitution progress can be traced spectroscopically by monitoring the growth of the new pigment's absorption peak as well as the appearance of an absorbance due to the free chromophore being introduced.

The analogue protein will revert back to its native state over prolonged periods of storage due to the chemical degradation of the oxime back to retinal and $\text{NH}_2\text{OH}\cdot\text{HCl}$, and the former will compete with the analogue chromophore for the binding site.⁸⁵ Complete removal of the retinal-oxime is therefore critical, but not easy. This can be accomplished by resuspending the analogue protein in a solution of BSA (Bovine Serum Albumin), followed by incubation and centrifugation. BSA will competitively solubilize the retinal oxime that is embedded within the membrane and will also effectively remove free analogue chromophore from the pigment. Repeated centrifuge washes will remove BSA once the protein has been purified of all chromophore contaminants. The reconstituted synthetic pigment can now be purified via standard methods (see section 3.1. and refs 74 and 98). As one reviewer of this manuscript noted, complete bleaching of the wild-type protein is rarely possible, and thus a small amount (~2%) of the native chromophore is typically present after all of the above procedures are carried out. This problem is unlikely to be catastrophic for materials-based studies but can be a major source of error when a small amount of the native protein dominates the spectroscopic or photochemical properties.

3.5. Chemical Modification and Organic Cation Substitution. Chemical modification is often used to stabilize one or more of the bacteriorhodopsin photocycle intermediates, typically the M or O states. The M state lifetime can be enhanced by high pH, dehydration, and the addition of amine compounds, all of which impact proton mobility within the protein. Profound effects are observed in dried polymer-based films of purple membrane that have been treated with organic amines [e.g., diaminopropane (Sigma D2360-2) or guanidine hydrochloride (Sigma G 7153)]. In such films, the lifetime of the M state can be prolonged by several orders of magnitude (from microseconds to minutes). However, most of the chemicals decrease the photochemical stability of the protein.

The O state lifetime can be prolonged by inhibiting proton release via pH adjustment to 6–6.5 and adding glycerol.^{75,99,100} An alternative approach is to replace the Mg(II) and Ca(II) metal cations in the protein with certain organic cations (see section 6.2 for examples). The first step is to remove the cations by using EDTA (Sigma E 9884) or cation-exchange resins (BioRad AG MP-50 Resin).^{55,77,88,101} The organic cations are then added to the solution or the polymer matrix in the form of salts.⁵⁴

3.6. Thin and Thick Film Holographic Media. Holographic films are prepared by using poly(vinyl alcohol) (PVA) (Aldrich, 36313-8), optical-grade gelatin (Sigma No. G-9382), or blends containing both polymers. BR, either freeze-dried or in the form of a pellet produced by centrifugation, is added to a PVA

solution, which is then sonicated and filtered to break up protein aggregates or diminish the size of the purple membrane fragments below 200 nm. Gelatin and chemicals (section 3.5) are then added to the solution as appropriate. The solution is then centrifuged mildly in a desktop unit, to remove bubbles that form during sonication and filtration.

To decrease the formation of density gradients during drying, it is important to maximize the surface area-to-volume ratio of the solution applied to the glass. This is done by using either spin coating (film thickness $<30 \mu\text{m}$) or an applicator blade (film thickness $>10 \mu\text{m}$). In the latter technique, the protein plus polymer solution is pulled out over the substrate by the use of a precision applicator blade (casually referred to as a Doctor Blade). By making a base into which the glass substrates fit, and then pulling the solution over the entire surface, one eliminates the meniscus and subsequent edge effects. The height of the blade is adjustable by a pair of micrometer actuators. However, the thickness of the dried film is many times smaller than that of the applied solution. Because humidity has a profound effect on the film properties, it is necessary to dry the films in a clean (class 50–200) chamber capable of regulating the relative humidity at a desired level. The films are then sealed while inside the chamber by using the retainer assembly shown in Figure 7. Examples of films and cuvettes are shown in Figure 8.

3.7. Polymer Cuvettes for Data Storage. Fabrication of BR-based optical cuvettes is accomplished by in situ polymerization of the acrylamide–bR solution [poly(acrylamide) Fisher BP1406-1]. The optical density of the purple membrane is adjusted to values ranging from 2 to 3 prior to polymerization. Several steps are taken to ensure low light scattering, including filtration and sonication, as well as addition of refractive index matching agents such as glycerol. The solution is quickly mixed and transferred to a standard fluorescence cuvette. Optimal results are obtained when the solutions are vacuum degassed and polymerized under reduced pressure using the apparatus shown in Figure 7b. The cuvette is sealed by using a UV-curable optical adhesive (Tra-Bond BiPax BA-2114). Examples are shown in Figure 8.

3.8. Systems Prototyping. We adopt here the nomenclature for prototyping that is common in industry. Prototypes are divided into three categories based on the primary goals. Level I prototypes seek proof of principle and are normally constructed in large scale format without concern for the overall size or cost of the system. Most of the components of these prototypes are re-usable, and include large frame lasers, computer-based data loggers, and optical mounts designed for large optical table mounting. A level I prototype is viewed as successful if one has demonstrated the feasibility of the methods and procedures inherent in the design. Level II prototypes investigate aspects critical to potential commercialization, with an increased emphasis on reliability, cost, and miniaturization. Multiple level II prototypes are common, with each version testing a specific design issue that must be solved prior to commercialization. Level III prototypes are near-final versions of the device that mimic as closely as possible the commercial version and are often made in sufficient quantity to permit beta testing by the intended audience. We provide examples of both level II and level III prototypes below.

4. Fourier-Holographic Associative Processors

Associative memories operate differently from the serial memories that are common in current computer architectures. These memories take an input data segment (or image) and

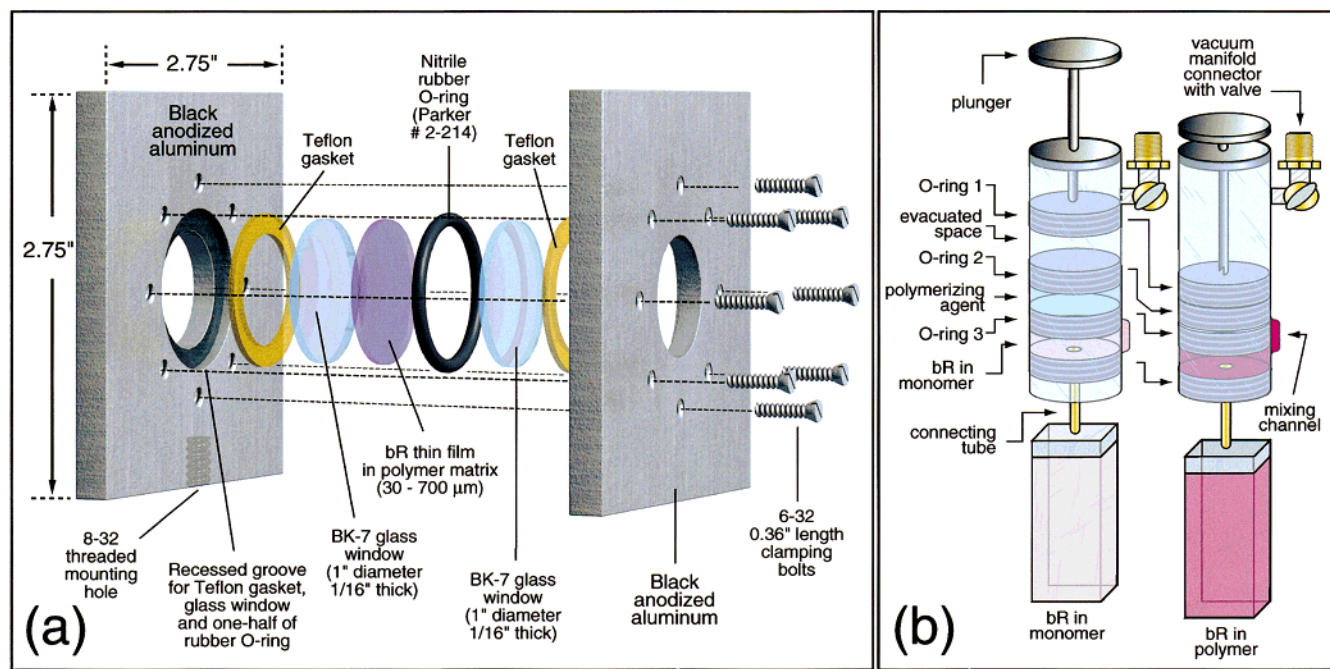


Figure 7. The reusable retainer for preparing sealed holographic thin and thick films is shown at left. The protein film is normally formed and dried on the BK7 glass substrate by using a Doctor blade and then sealed under controlled humidity inside the retainer (section 3.6). The same retainer allows different film thicknesses by selecting Teflon gaskets of the appropriate thickness. The fixture for preparing degassed memory cuvettes is shown at right. This apparatus has also been used to prepare cuvettes in microgravity on two Space Shuttle flights (STS-54, January 1993; STS-69, September 1995). Rigorous degassing is critical for microgravity polymerization to prevent the formation of suspended bubbles.

independently “scan” the entire memory for the data block that matches the input. In a majority of implementations, the memory will find the closest match if it cannot find a perfect match. Finally, the memory will return the data block in memory that satisfies the matching criteria. The most sophisticated associative memories permit variable sized blocks, so that the association process is flexible with respect to the amount of information returned. Because the human brain operates in a neural, associative mode, the implementation of large capacity associative memories will likely be a necessary component of any computer architecture that achieves artificial intelligence.

Fourier transform optical associative memories have significant potential for applications in optical computer architectures, optically coupled neural network computers, robotic vision hardware, and generic pattern recognition systems.^{36,56,102,103} Our current design is shown in Figure 9 and is based on the modification of an architecture proposed originally by Paek and Psaltis.¹⁰³ Our modifications have been introduced with two goals in mind. The first is that we seek to have all the input and reference data introduced via a single active matrix liquid crystal spatial light modulator (AMSLM), so that the system can be operated entirely without external optical coupling. Second, the memory has been redesigned so that it can be miniaturized onto a single PCI (Peripheral Component Interconnect) computer card. The background to these designs has been discussed in detail.^{7,30,104} Our goal here is to use this memory as an example of a holographic system, and the role of prototyping in the development of protein-based hardware.

The optical diagram shown in Figure 9 illustrates the use of the memory to associate a small reference database of four faces. Naturally, a useful memory would operate with a larger database and would not be limited to images. We will return to these issues after describing the operation of the memory on the simple example reference set. Before the memory can be used, the database must be stored on the protein holographic films. The data are stored as standard, and high-frequency enhanced,

Fourier transforms at each location for which a pinhole aperture is located. That is, each image is associated with an individual pinhole along the optical axis, and is located on the reference planes by reference to that pinhole axis. The easiest way to do this is to write the images by opening only one pinhole at a time, but higher speed, lower resolution operation can be accomplished by writing all the images at once. The lifetime of the holographic film must be adjusted accordingly, and while D96N films are optimal for speed, D96N + chemical additives or blue variant films (section 2.4) are usually required for handling large databases. During the readout operation, the input image is read into the loop by using the same spatial light modulator used to write the reference images. The Fourier transformed product of the image reference is formed and retransformed at the plane of a pinhole array (PHA). The resulting correlation patterns are sampled by the pinholes (diameter $\sim 500 \mu\text{m}$) which are, by the nature of the optical design, precisely aligned with the optical axis of the reference images (one pinhole per reference page). Light from the pinhole plane is retransformed and superimposed with the reference image stored on bacteriorhodopsin hologram 2 [H2]. The resulting cross correlation pattern represents the superposition of all images stored on the multiplexed holograms and is fed back through the threshold modulator for another iteration. Thus, each image is weighted by the inner product between the pattern recorded on the input AMSLM from the previous iteration and itself. The output locks on to that image stored in the holograms, which produces the largest correlation flux through its aligned pinhole.

During the process of sampling the correlation patterns, it is interesting to note that the inclusion of the pinholes destroys the shift invariance of the optical system. If the input pattern is shifted from its nominal position, the correlation peak shifts as well, and the correlation light flux will miss the pinhole. Thus, the pinholes not only limit the flexibility of the system but also require that the reference data be stored at precise locations

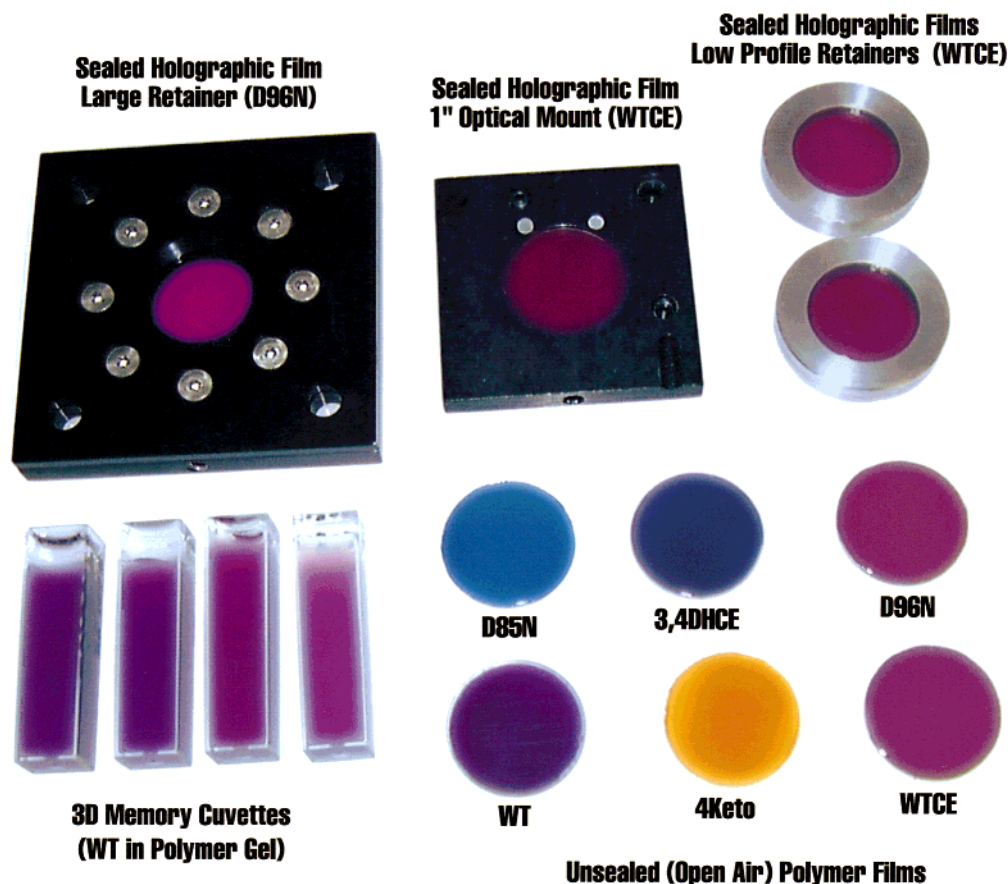


Figure 8. Examples of thin films and memory cuvettes based on bacteriorhodopsin. The retainer shown in the upper left is detailed in Figure 7a. The smaller retainers shown at upper middle and upper right are compression type, and not reusable. The following codes are used: D96N (Asp-96 \rightarrow Asn-96), WT (wild-type), WTCE (wild-type chemically enhanced), D85N (Asp-85 \rightarrow Asn-85), 3,4DHCE (3,4 dehydro retinal (or A2 retinal) with chemical enhancement), 4Keto (4-keto retinal). All films are poly(vinyl alcohol) based. The memory cuvettes are pH adjusted polyacrylamide with index matching additives.

within the two holographic films. Indeed, this problem has been identified as an inherent flaw in such designs. We have adopted this design, however, to avoid ghost images that are inherent in free-spatial-associative designs. The pinholes also have the advantage of allowing precise alignment of the reference images, by replacing the fixed pinholes with electrically addressable pinholes (i.e., low-resolution active matrix liquid crystal spatial light modulators). Our architecture was designed to facilitate miniaturization of the entire optical system onto a single memory card, as shown in the level III prototype design compared to a semiconductor version in Figure 10. We emphasize that this is a CAD picture and that this associative memory card has not yet been prototyped.

Our memory design does not automatically correct for variation in the size of the input pattern, nor is the associative process invariant to translation or rotation of the input image or data set. This problem is inherent to all comparable optical correlators, although there are a number of optical tricks that have been proposed to handle translational or rotational shifts. For example, we can take advantage of the fact that our input data are entered via an electronically addressed spatial light modulator. Thus, we can use the computer controller to adjust the input image on the basis of the type of input. All textual data will be converted to the same font and font size, and all text will be stored and presented horizontally. An excellent demonstration of textual association has been reported by Hampp and co-workers.³⁶ One inherent advantage of Fourier association is that images, binary data, and textual data can be combined on the same reference page and be associated with

fragments of these data. So long as the binary data are represented in redundant (bit symmetrical) format, the text data are adjusted as previously described, and the image data are size and orientationally corrected, fragments of any subsets of these can trigger correct associative output.

5. Three-Dimensional Branched-Photocycle Memories

Advances in central processor technology have altered the character of computer technology from processor-limited toward memory-limited performance.³² The overall throughput of many scientific and image analysis problems is now determined primarily by the size and data transfer bandwidths of the random access memory rather than the speed of the central processor unit or the floating point hardware. This situation has generated an increased awareness that new memory architectures providing more cost-effective storage capacities, local processing capabilities or data bandwidths should be investigated.¹⁰⁵ Three-dimensional memories store information in a volumetric memory medium and offer as much as a 1000-fold improvement in data storage capacity for a given enclosure size, although optical and reliability considerations tend to reduce the comparative advantage factor to values closer to 300.^{106–109} The two most common architectures are based on two-photon^{105–108, 110} or holographic^{103,111,112} methods. The branched-photocycle architecture explored here represents an alternative approach that offers some important advantages. First, the use of temporally separated excitation processes rigorously excludes photochem-

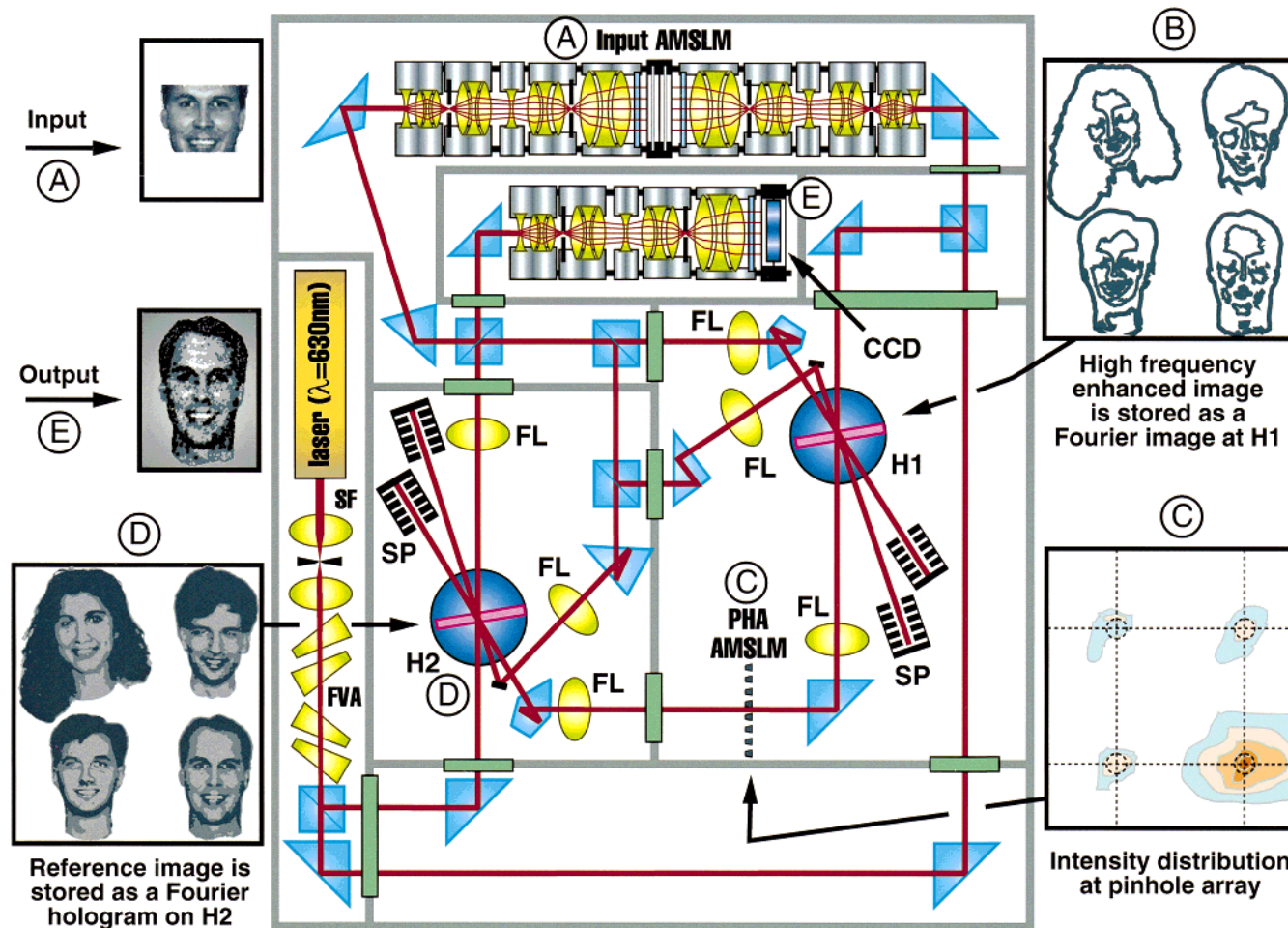


Figure 9. Schematic diagram of a Fourier transform holographic (FTH) associative memory with read/write FTH reference planes using thin polymer films of bacteriorhodopsin to provide real-time storage of the holograms. Note that a partial input image can select and regenerate the entire associated image stored on the reference hologram. Although only four reference images are shown, an optical associative memory can store many hundreds or thousands of images simultaneously. This memory can also work on binary data by using redundant binary logic, and a small segment of data can be used to find which page has the largest association with the input segment. Selected components are labeled as follows: AMSLM, active matrix spatial light modulator; FL, Fourier lens; FVA, Fresnel variable attenuator; H1, H2, protein-based holographic films; PHA/AMSML, computer reconfigurable pinhole array; SF, spatial filter; SP, beam stop.

istry outside of the doubly irradiated volume, which simplifies the optical design and improves reliability. Second, the use of linear rather than nonlinear excitation allows the use of inexpensive CW lasers, which increases flexibility and decreases the cost of the read/write architecture. [However, the lack of inexpensive blue erase lasers may postpone commercialization of high-speed versions (see below).] The total memory system gains additional comparative advantage from the inherently low cost of the storage medium.

The branching reaction that we exploit was introduced in section 2.3 and is shown in Figure 1b. The memory functions by assigning the resting state (bR) to bit 0 and both P and Q to bit 1, as shown in Scheme 3.

Scheme 3 indicates the wavelength maximum (in nanometers), the conformation, and the protonation state of the chromophore directly underneath the intermediate label. There are two side reactions that decrease potentially the yield of the O state, and when examining bacteriorhodopsin for device applications, we refer to these as shunts. The $L \rightarrow bR$ shunt is observed at lower temperatures and in some mutants and is easily avoided.^{113,114} The $N \rightarrow bR$ shunt is competitive with the $N \rightarrow O$ reaction in the wild-type.^{47,115,116} The diminution or removal of this shunt is a major goal of our chemical and genetic efforts. Shunt 2 occurs after the proton has been pumped and

would increase the efficiency of the proton pumping process. Natural selection would likely favor mutations that enhance shunt 2, and we anticipate that mutations exist which significantly decrease this side reaction, and a few candidates have already been found (see below).

A random access memory must be able to write, read, and erase data, and each of these operations is described in a separate section below. The timing protocols of the read and write processes are shown in Figure 11. A schematic diagram of the key optoelectronic components of a level II prototype are shown in Figure 12.

5.1. Data Are Written in Parallel via a Branching Reaction. The initial process in both writing and reading is the selection and activation of a thin segment of protein within the volumetric memory medium. This thin activated region is called a page, and the activation process is called paging. The thickness of the page is dependent on the optical arrangement and varies from an rms value of $15 \mu\text{m}$ (multiple prism system) to $100 \mu\text{m}$ (simple cylindrical lens). Data are then written by using an orthogonal beam of light that is shifted in time so that it photoactivates the O state (Scheme 3). The process is explicitly documented on the left-hand side of Figure 11 for a process that writes three bits within the page. The vertical axis of Figure 11 charts nominal time relative to the firing of the page

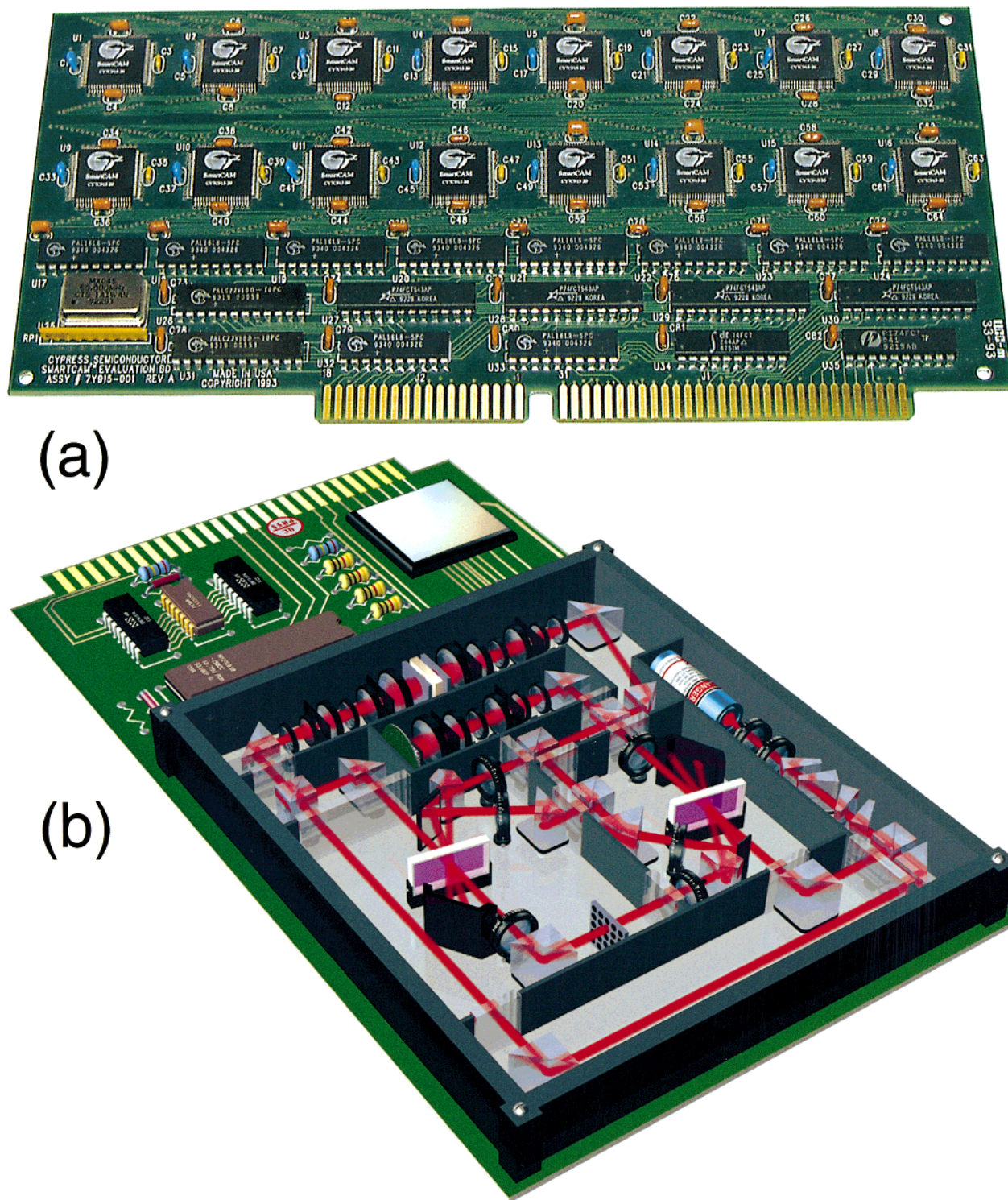


Figure 10. The top picture (a) shows a level III (beta test) prototype of a semiconductor associative memory manufactured by Coherent Research Inc., Syracuse, NY. This memory provides single clock cycle binary association for a database of 16 384 64 bit words. The schematic below (b) shows a proposed level III Fourier holographic optical associative memory based on two bR thin films. This memory would handle simultaneously both character and image data and provide 1024 pages of 65 536 bits each. A full associative search would be done in 40 ns.

addressing (or *paging*) laser. Two milliseconds following paging, the data laser and the data beam spatial light modulator are activated ($\lambda = 680 \text{ nm}$, $\Delta t \approx 3 \text{ ms}$) to irradiate those volume elements into which 1 bits are to be written. This process converts O to P in these, and only these, voxels within the memory cuvette. (A voxel is the volumetric pixel formed in the volume element created by a single write pixel overlap with the active page.) After many minutes the P state thermally decays to form the Q state (section 2.3 and Figure 6). The write

process is accomplished in $\sim 10 \text{ ms}$, the time it takes the protein to complete the photocycle.

The combination of a paging and write beam are shown at the top of Figure 12. Note that these beams are not turned on simultaneously but are shown simultaneously for convenience. The use of a prism system for creating a narrow page beam provides near-diffraction limited performance, but at the expense of complexity. Alternative approaches are under investigation (see below). All designs use paging optics on both sides of the

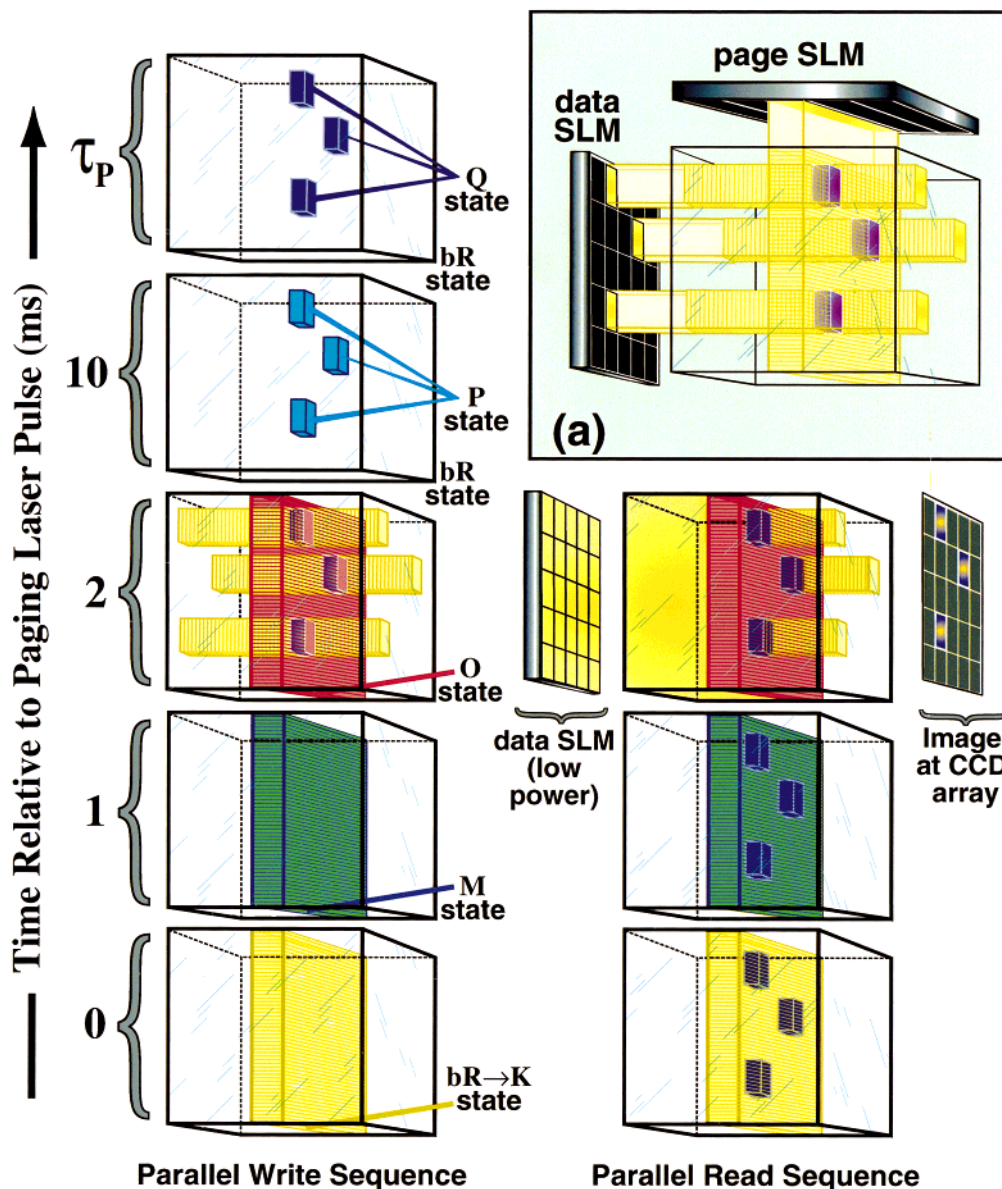
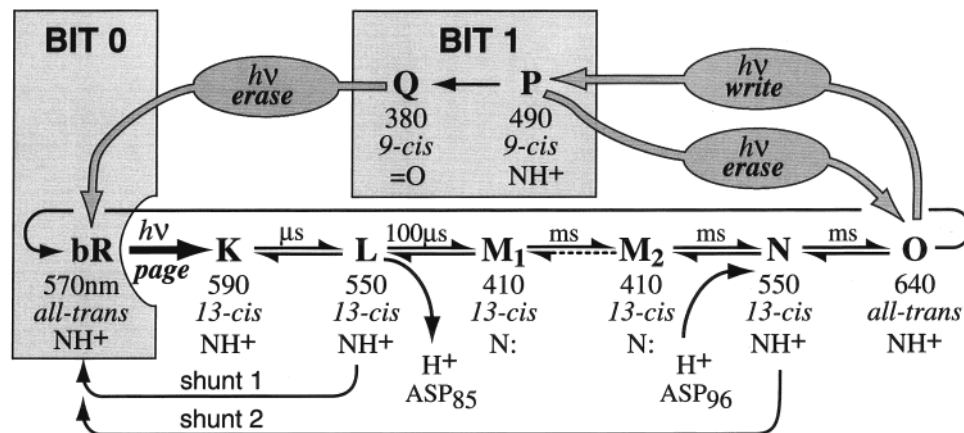


Figure 11. Parallel write sequence (left) and parallel read sequence (right) for the hypothetical storage and retrieval of three bits of data in a page of memory using the branched-photocycle architecture (see text).

SCHEME 3



data cuvette to enhance resolution, photocycle conversion, and homogeneity. Only one side of the paging optics is shown in Figure 12 for convenience.

The above description describes the process of writing a single

bit per voxel, but methods are available that enhance storage density. We discuss those options in more detail below.

5.2. Data Are Read in Parallel by Using Differential Absorptivity. The read process takes advantage of the fact that

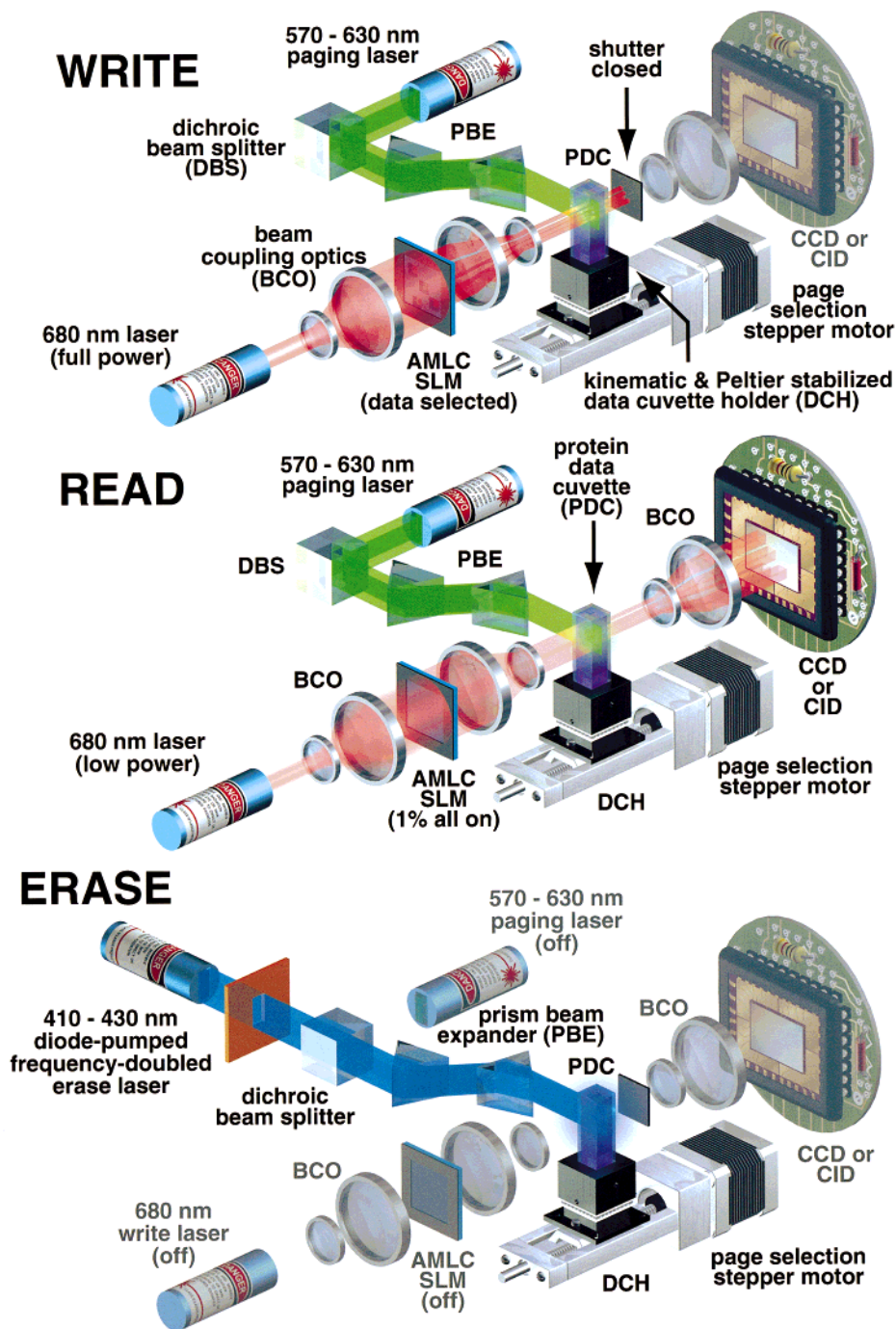


Figure 12. Read, write, and erase processes based on a level I prototype design (see text).

light of wavelength around 680 nm is absorbed effectively by only two intermediates in the photocycle of light-adapted bacteriorhodopsin, the primary photoproduct K and the relatively long-lived O intermediate (see Figure 2). If the light beam is timed properly, the K state can be avoided and only the O state will absorb light. This is the approach that is used to image data within an activated page, as shown on the right-hand-side of Figure 11.

The read sequence starts out in a fashion identical to that of the write process by activating the paging beam. After 2 ms, the data laser and the data SLM are turned on, but at a low constant power (roughly 1% of nominal write intensity). This process images the active page onto the CCD detector. Those elements in binary state 1 (P or Q) do not absorb the 680 nm light, but those volumetric elements that started out in the binary 0 state (bR) absorb the 680 nm light, because these elements

have cycled into the O state. (It is purely coincidental that the "O" molecular state is used to monitor the "0" binary state.) Noting that all of the volumetric elements outside of the paged area are restricted to the bR, P, or Q states, the only significant absorption of the beam is associated with O states within the paged region. The CCD detector array therefore observes the differential absorptivity of the paged region, and the paged region alone. This selectivity is the key to the read operation, and it allows a reasonable signal-to-noise ratio even with thick (1–1.6 cm) memory media containing $>10^3$ pages. Because the absorptivity of the O state within the paged region is more than 1000 times larger than the absorptivity of the remaining volume elements combined, a very weak beam can be used to generate a large differential signal. The read process is complete in about 6 ms, but a second read cannot be carried out until the photocycle has completed thereby limiting multiple read proc-

esses to 10 ms cycles. Each read operation must be monitored for each page, and a refresh operation performed after ~ 1000 reads. The three most recent pages are stored in semiconductor cache memory to minimize the number of refresh operations.

5.3. Data Can Be Erased by Page or Globally. The P and Q states can both be photoconverted back to bR by using blue light (Figure 1b; Scheme 3). If one has access to coherent light, then individual pages can be cleared by using irradiation at or near 410 nm, a wavelength that intercepts both P and Q (Figure 2). Our early prototypes used the 413 nm output of a krypton-ion laser. Such an approach is only useful for level I prototypes, however, and our various level II prototypes are investigating three alternatives. The first is a frequency-doubled diode laser manufactured by NanoLambda Corp., Kerhonken, NY (Figure 12). Other than cost, this approach is adequate and will suffice until blue diode lasers are available. Alternatively, one can clear an entire data cuvette by using incoherent light in the 360–450 nm range. We explore this approach in the prototype described below. A broad-band data clear operation must be carried out in the absence of red light, however, because blue light can activate the photocycle and produce the O state. As one reviewer noted, however, the O state does have appreciable absorptivity in the 360–450 nm range. This situation does not cause a problem, however, because the absence of red light limits the population of O state molecules to the small amount generated by photochemical conversion of P. Because the P and Q states are preferential absorbers of the erase beam, the end photostationary state distribution favors bR by factors of many hundreds, and erasure is efficient. Erasure does not have to be perfect, however, for the memory to work properly. The use of differential absorptivity data read methods (section 5.2) allows for an inherent background level of P and Q.

6. Optimizing the Protein for 3D Data Storage

Although the native protein can be used in the branched-photocycle architecture, the low quantum yield of the O to P photoconversion ($\sim 2 \times 10^{-4}$) coupled with the relatively poor yield of the O state ($\sim 3\%$ under ambient conditions) suggests that significant improvements can be made in the wild-type protein for this application. Indeed, as has been noted, evolution would likely converge on a protein sequence and structure that minimizes the probability of branching, because the formation of Q could be terminal. Fortunately, much can be done to improve the efficiency of the branching reaction, and this section outlines some of the methods that are under study to enhance the yield of the O state and the quantum efficiency of the $O \rightarrow P$ photoreaction. This section represents a progress report rather than a final recipe for optimization. Much work remains to be done with respect to protein optimization.

6.1. Temperature and pH Effects. Detailed kinetic and pH studies have shown that the amount of O state that is formed is very sensitive to both temperature and pH.^{42,115–117} The temperature effect is clearly shown in Figure 13. We enhance O state formation by using Peltier devices to maintain the temperature of the memory cuvette at 35 °C. Similarly, the pH of the memory medium is adjusted to pH 6 prior to polymerization to enhance O. The simple combination of these two effects enhances O state formation by factors of 2–3 relative to ambient temperature wild-type.

6.2 Chemical Optimization. We discovered quite by accident that organic cations have a significant impact on the lifetime and yield of the O state.⁵⁴ This replacement is accomplished as described in section 3.4. At first, we believed that the organic cations entered a chromophore adjacent cation binding site (see

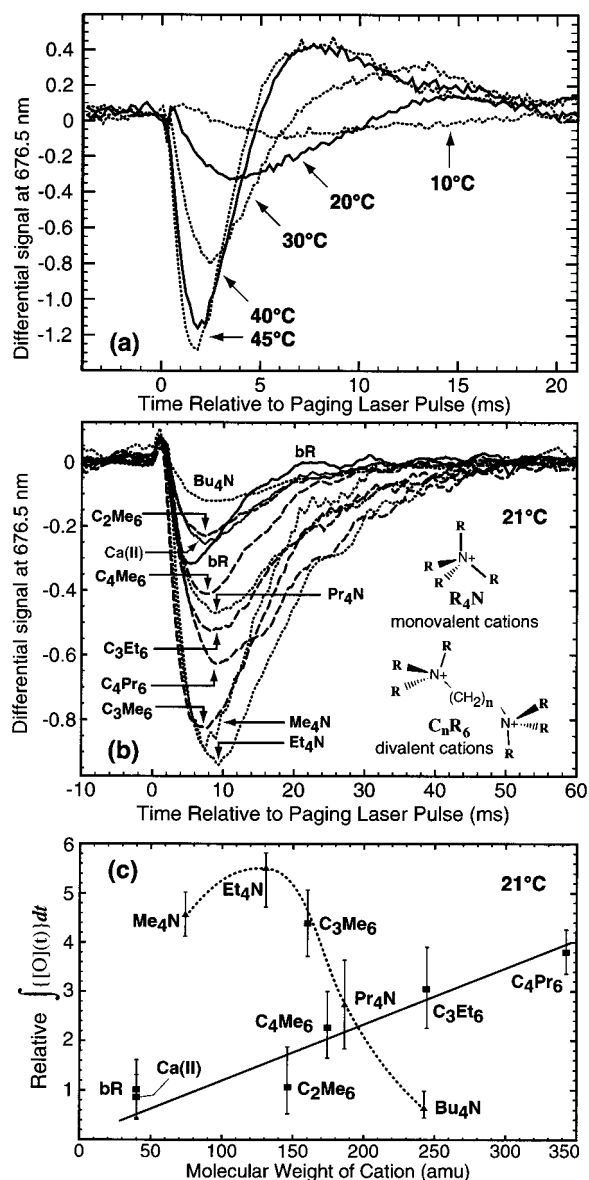


Figure 13. Effect of temperature on the read signal due to absorption by the O state of light at 676.5 nm (a) and the influence of organic cation size and structure on the formation, decay, and yield of the O state (b and c). As shown in (a), increasing temperature enhances the formation of the O state. As shown in (b) and (c), some organic cations enhance the yield and/or the lifetime of the O state. The efficiency of photogenerating the P state from the O state (i.e., writing bit 1) is proportional to the integral of O concentration with respect to time, which is graphed as a function of the cation molecular weight in (c).

ref 54), but more recent studies suggest that these organic cations are occupying sites closer to the surface.^{48,117,118} The mechanism is not well understood, but as can be seen in Figure 13, the organic cations can have a large impact on the yield of the O state without increasing the lifetime of the O state significantly. Our best results are obtained by using monovalent organic cations (Me₄N or Et₄N), pH control (6.5), glycerol additives, and a working temperature of 35 °C.

6.3. Site directed mutagenesis coupled with pH and chemical manipulation will ultimately provide the best control over the efficiency of the branching reaction. In general, any mutant that enhances proton availability and mobility from the cytoplasm into the binding site and which decreases access of the proton on Asp-85H to the extracellular domain will likely enhance the formation of the O state. However, a majority of mutants for which the O state yield is enhanced increase the lifetime of the

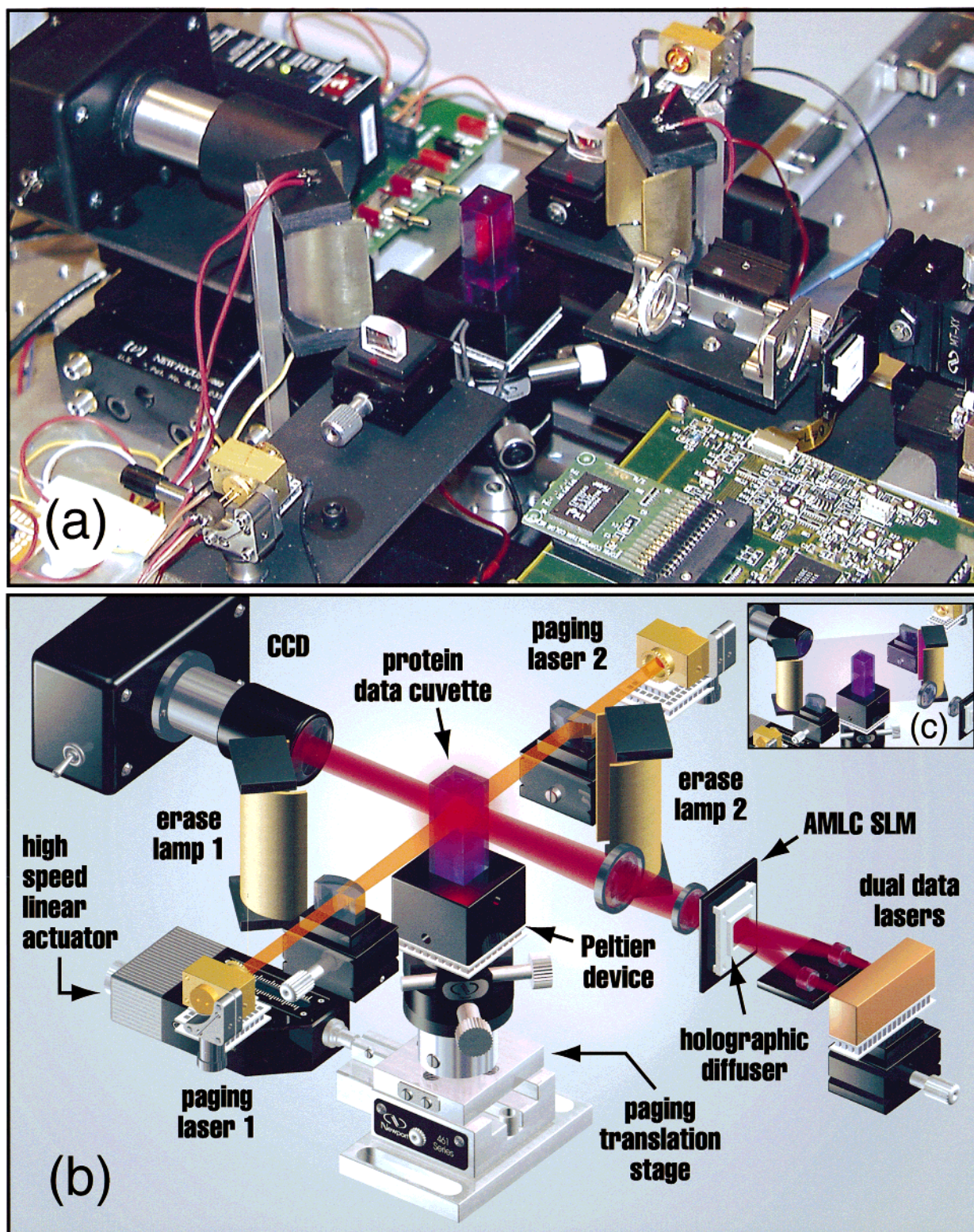


Figure 14. Close-up picture (a) and a schematic (b) of the current level II prototype of the branched-photocycle volumetric memory. Key components of the prototype are shown and labeled in the schematic (b). This prototype uses a global erasure of the entire data cuvette via activation of a pair of cylindrical UV lamps. The lamps are located at the focus of two cylindrical hyperbolic mirrors positioned so that the entire memory cuvette can be irradiated (inset c). Dual data lasers coupled to the active matrix liquid crystal spatial light modulator (AMLC SLM) via a holographic diffuser are used to generate noncoherent light so that the imaged data beam does not contain diffracted artifacts (see text).

O state beyond that useful for implementation in a branched-photocycle memory. The following mutants have been studied to date: R82A, R82C, R82K, L93A, L93T, V49A, E204Q, E204D, E194Q, E194D, Y185F, and F208N and the double mutants E194Q/E204Q and E194D/E204D. [Selected amino acid abbreviations are alanine (Ala, A); arginine (Arg, R);

asparagine (Asn, N); aspartic acid (Asp, D); cysteine (Cys, C); glutamine (Gln, Q); leucine (Leu, L); lysine (Lys, K); methionine (Met, M); phenylalanine (Phe, F); threonine (Thr, T); tyrosine (Tyr, Y).] A majority of these mutants have been prepared and studied previously, although the goals were not data storage but rather a better understanding of structure and

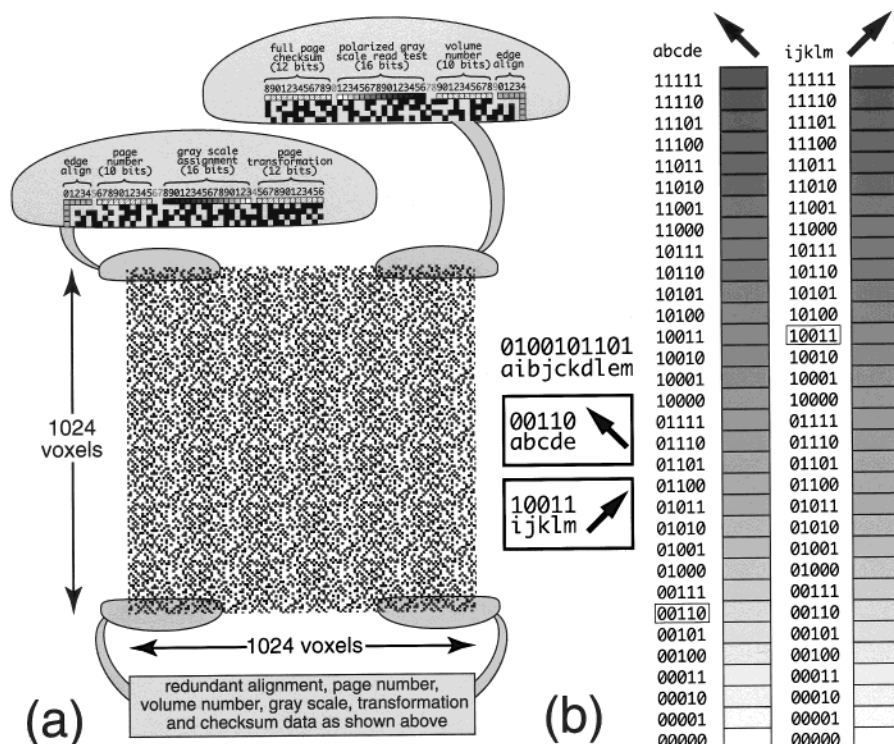


Figure 15. Each page of data consists of a rectangular array of voxels, where each voxel can be assigned to store a single bit, or many bits, by using polarization and gray scale multiplexing. Our preliminary design for a page includes registration (optical alignment), page number, volume number, gray scale, transformation, and checksum data along the edges (a). Current multiplexing schemes seek to store 10 bits in each voxel based on the use of two orthogonal polarizations and 16 density levels, as shown in (b).

function.^{117,119–129} We have reexamined the R82 mutants^{125–127} to investigate the role of Arg-82 motion during the latter stages of the photocycle (see Figure 9 of ref 48), and to determine the extent to which Arg-82 mutants (with the addition of guanidine where necessary to maintain function) can control O state properties. To date, no Arg-82 mutant has been found that enhances O state yield significantly. Mutations involving Leu-93 are known to enhance O state formation,^{122,128} but our studies indicate that these mutations generate an O state with a decreased quantum efficiency of $O \rightarrow P$ photochemistry. To date, the best results have been obtained by using single and double mutations involving Glu-194 and Glu-204.^{123,129–134} These mutations appear to enhance both the yield of O and the quantum efficiency for $O \rightarrow P$ photochemistry, but no mutant has performed as well as the chemically enhanced protein system described in section 6.2.

7. Prototyping and Reliability Studies

The 3D volumetric memory based on the branched-photocycle is in a second generation of prototyping, and the current level II prototype is shown in Figure 14. (The previous design is shown schematically in Figure 12 and described in section 5.) In this section we describe the principal features of the current prototype and why these features were implemented. We close this section by presenting read error histograms that provide a well-defined measure of the reliability of the prototype architecture.

The present prototype seeks to provide a lower resolution, more compact, and more reliable memory. This memory has been designed in a modular fashion so that individual components can be rapidly replaced so that new component subsections can be tested quickly. All of the electronics associated with the memory are now board-based rather than computer-based,

although the firmware associated with many of the controller boards is externally programmable. The key features are discussed below.

Dual paging lasers are used to provide homogeneous page activation. Although 570 nm lasers would be optimal, we are using two 60 mW, 630–635 nm lasers because relatively inexpensive diode lasers are available with these specifications. We convert $\sim 25\%$ of the molecules within the irradiated page to the O state, in preparation for either writing or reading.

Holographically coupled dual data lasers are implemented in this prototype to deal with an interesting problem associated with small pixel-sized active matrix liquid crystal spatial light modulators (AMLC SLMs). The use of such SLMs to control coherent light sources generates pixel aperture interference that is otherwise absent with incoherent sources. This problem has been reduced to acceptable levels by using two data lasers that are coupled via a pair of lenses to a holographic diffuser, as shown in Figure 14. The coupling of two lasers removes the coherence inherent in single laser sources, and the holographic diffuser provides an even intensity distribution across the surface of the modulator. We use two 50 mW 680 nm diode lasers. The high power is required because of the low quantum efficiency of the $O \rightarrow P$ photochemistry (see discussion above). If the native protein is used, only about $\sim 1\%$ of the protein can be converted from bR to Q. Organic cation analogues (section 6.2) or Glu-194/Glu-204 mutants (section 6.3) yield conversions that are 5–10-fold higher and approach the conversion levels that are necessary for reliable and efficient operation.

High-speed linear actuator. While it may appear inefficient to move the data cuvette rather than the optics, paging through cuvette translation is the preferred method when speed and reliability are taken into account. The data cuvettes are light (4.5 g plastic, 9.1 g BK-7), and the kinematic mount and the

Peltier device dominate the inertial weight. The prototype shown in Figure 15 uses a high-speed linear actuator (Newport 850F-HS) to locate the cuvette. This device allows the cuvette to be positioned on average in 60 ms, a value sufficient for the present testing purposes. Ultimately, we will use linear magnetic motors to achieve 10 ms latencies.

Global erasure of the entire data cuvette is achieved via activation of a pair of cylindrical UV lamps (All Electronics, UV-325 + BXA 12576), which have outputs of 463 ± 40 nm. This soft UV light couples adequately to the absorption spectra of both P and Q and sets all the bits within the entire memory cuvette to state zero (bR) in a few minutes. The lamps are located at the focus of two cylindrical hyperbolic mirrors and are collimated as shown in Figure 14c so that the entire memory cuvette is irradiated when properly positioned.

Multiplexing of the data to achieve higher storage density is implemented by using a single polarization version of the gray scale and polarization multiplexing scheme shown in Figure 15. This scheme stores 10 bits per voxel, and the use of a single polarization provides 5 bits per voxel. Multiplexing is an important component of 3D data storage as it achieves viable storage densities without the need to operate near the diffraction limit. The spatial light modulator (Kopin, 320C) and the CCD detector (Cohu 1100) are designed to provide 8-bit gray scale capability, which yields the potential of multiplexing 16 bits into each voxel via polarization doubling. In practice, reliability limits the writing and reading processes to 5-bits per polarization, leading to the 10-bits/voxel inherent in the scheme shown in Figure 15. In addition, a number of bits along the edges must be allocated to alignment and checksum information. With these features fully implemented, a standard $1 \times 1 \times 3$ cm³ data storage cuvette can store approximately 10 gigabytes. This storage capacity translates to the use of between 10^4 and 10^5 protein molecules per bit for typical protein concentrations utilized here and provides an adequate number of molecules-per-bit to yield a statistically relevant ensemble as required to maintain reliability (see below).¹³⁵

Error analysis is carried out by measuring read histograms, examples of which are shown in Figure 16.⁴³ A detailed discussion of error sources and error analysis for 3D memories is beyond the scope of this study, and we direct the reader to ref 43 for a more comprehensive discussion. Briefly, we note that a read operation carried out via differential absorption is measured on a normalized scale where 0 is low intensity reaching the detector (bit 0, O state absorption) and 1 is high intensity reaching the detector (bit 1, P and Q present and less O state absorption). By using a differential read process as shown in Figure 11, the detector and associated circuitry normalize the signals across the detector array so that under perfect conditions and no error, the two histograms would yield only two peaks at 0 and 1. In practice, you get results as shown in Figure 16. A perfect read process is not necessary, however, so long as there is no overlap between the bit 0 and bit 1 histograms, and a single threshold can be assigned that does not shift with changes in the location or data distribution of the page. As can be seen, however, the early prototype had considerable bit assignment error due to histogram overlap. The overlap error is improved in the more recent prototype, but the threshold shifts with data distribution. The current error levels are quite unacceptable, but we anticipate no problems in dramatically improving the reliability of the memory as in the optics, electronics, and materials undergo systematic improvement.

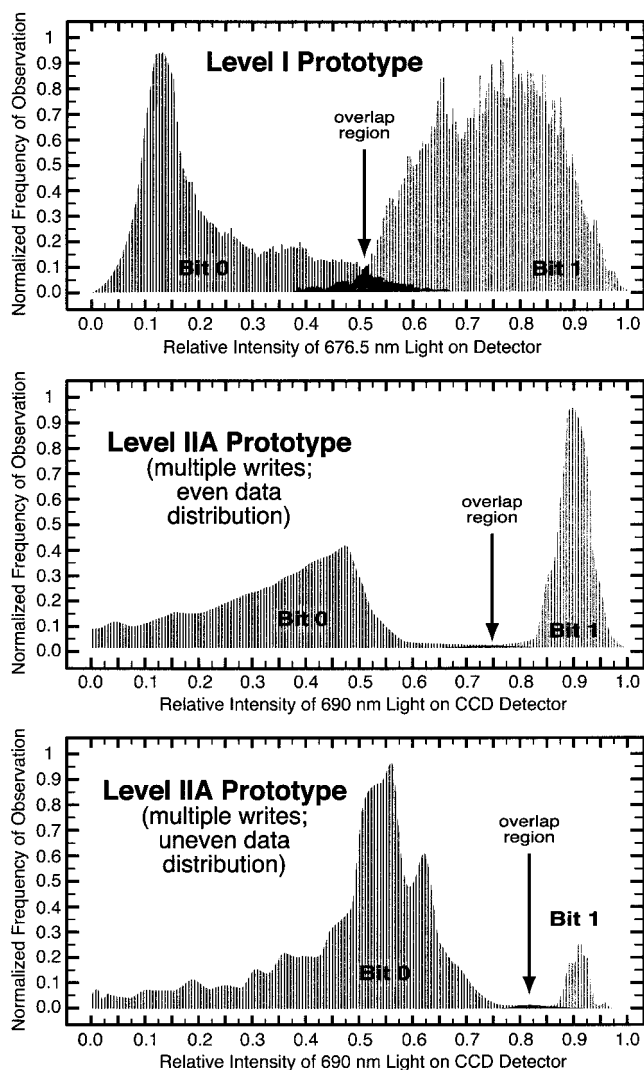


Figure 16. Reliability of data storage is analyzed on the basis of the generation and analysis of read histograms. The top histogram was generated using an early prototype, and the bottom two were generated using a more advanced prototype. While improvement is noted, further work is required to achieve acceptable levels of reliability. The probabilities of a read error for the above three histograms are 0.044 (top), 0.009 (middle), and 0.011 (bottom). Adapted from ref 43.

8. Concluding Remarks

It remains to be seen whether any of the devices described here will have a commercial future. Nevertheless, we hope the above discussion has fostered an appreciation for the potential of protein-based devices in computer architectures. We close this article by addressing an interesting question that is often posed to scientists and engineers working on bacteriorhodopsin devices. Namely, is there something unique about bacteriorhodopsin that makes it the ultimate bioelectronic material, or has the early Soviet research into bacteriorhodopsin devices generated sufficient inertia to cause an unjustified preoccupation with this protein? We believe that both statements are correct. Bacteriorhodopsin is unique in providing a thermally stable, photochemically rugged, easily modified protein that can be used as the active component in a variety of photonic devices. The evolutionary development of a light-transducing protein that can operate in a salt-marsh bacterium selects a number of properties that are required for device applications of the type investigated here. But it is also true that far too little effort has been directed at investigating other proteins and that these alternative biomaterials may ultimately provide superior performance. We hope

that this article will help to stimulate not only continued interest in bacteriorhodopsin but a renewed interest in exploring other proteins for device applications.

Acknowledgment. The research in our laboratory was funded by grants from the National Institutes of Health (GM-34548), Air Force Research Laboratories (RL-97-230; F30602-98-C-0105), National Science Foundation (CHE-96-0022N) and the W. M. Keck Foundation. We thank Drs. Richard Needleman, Norbert Hampp, Dieter Oesterhelt, and Mark Braiman for providing us with vectors and/or mutants, Dr. John Spudich for providing the original overproducing strain, Drs. Janos Lanyi and Hudel Luecke for providing us with the 1brx and 2brx structures prior to submission to the protein data bank, and Dr. Charles Storman for providing a beta test unit of the CRi semiconductor associative memory (Figure 10a). We also thank Vagisha Sharma for preparing the graphics for this article, and Rob Herman and Connie Birge for technical support.

References and Notes

- (1) Keyes, R. W. Minimum Size Devices. In *Molecular Electronics – Science and Technology*; Aviram, A., Ed.; Engineering Foundation: New York, 1989; pp 197–204.
- (2) Birge, R. R. *Adv. Chem.* **1994**, *240*, 1–14.
- (3) Iwai, H. *IEEE J. Solid-State Circuits* **1999**, *34*, 357–366.
- (4) Vsevolodov, N. N. *Biomolecular Electronics. An Introduction via Photosensitive Proteins*; Birkhauser: Boston, 1998.
- (5) Greenbaum, E. J. *Phys. Chem.* **1990**, *94*, 6151–6153.
- (6) Boxer, S. G.; Stocker, J.; Franzen, S.; Salafsky, J. Re-engineering photosynthetic reaction centers. In *Molecular Electronics- Science and Technology*; Aviram, A., Ed.; American Institute of Physics: New York, 1992; Vol. 262, pp 226–241.
- (7) Birge, R. R. *Annu. Rev. Phys. Chem.* **1990**, *41*, 683–733.
- (8) Lee, I.; Lee, J. W.; Greenbaum, E. *Phys. Rev. Lett.* **1997**, *79*, 3294–3297.
- (9) Vsevolodov, N. N.; Poltoratskii, V. A. *Sov. Phys. Technol. Phys.* **1985**, *30*, 1235.
- (10) Bunkin, F. V.; Vsevolodov, N. N.; Druzko, A. B.; Mitsner, B. I.; Prokhorov, A. M.; Savranskii, V. V.; Tkachenko, N. W.; Shevchenko, T. B. *Sov. Technol. Phys. Lett.* **1981**, *7*, 630–631.
- (11) Grigorieff, N.; Ceska, T. A.; Downing, K. H.; Baldwin, J. M.; Henderson, R. *J. Mol. Biol.* **1996**, *259*, 393–421.
- (12) Stuart, J. A.; Birge, R. R. Characterization of the primary photochemical events in bacteriorhodopsin and rhodopsin. In *Biomembranes*; Lee, A. G., Ed.; JAI Press: London, 1996; Vol. 2A, pp 33–140.
- (13) Ebrey, T. G. Light energy transduction in bacteriorhodopsin. In *Thermodynamics of membrane receptors and channels*; Jackson, M. B., Ed.; CRC Press: Boca Raton, FL, 1993; pp 353–387.
- (14) El-Sayed, M. A. *Acc. Chem. Res.* **1992**, *25*, 279–286.
- (15) Oesterhelt, D.; Stoekenius, W. *Nature (London), New Biol.* **1971**, *233*, 149–152.
- (16) Lawrence, A. F.; Birge, R. R. Communication with submicron structures. Perspectives in the application of biomolecules to computer technology. In *Nonlinear electrodynamics in biological systems*; Adey, H. R., Lawrence, A. F., Eds.; Plenum: New York, 1984; pp 207–218.
- (17) Schick, G. A.; Lawrence, A. F.; Birge, R. R. *Trends Biotechnol.* **1988**, *6*, 159–163.
- (18) Birge, R. R.; Zhang, C. F.; Lawrence, A. F. Optical random access memory based on bacteriorhodopsin. In *Molecular Electronics*; Hong, F., Ed.; Plenum: New York, 1989; pp 369–379.
- (19) Mobarry, C.; Lewis, A. *Proc. SPIE* **1986**, *700*, 304.
- (20) Marwan, W.; Hegemann, P.; Oesterhelt, D. *J. Mol. Biol.* **1988**, *663*–664.
- (21) Sasabe, H.; Furuno, T.; Takimoto, K. *Synth. Met.* **1989**, *28*, C787–C792.
- (22) Hong, F. T. *Adv. Chem.* **1994**, *240*, 527–560.
- (23) Vsevolodov, N. N.; Druzko, A. B.; Djukova, T. V. Actual possibilities of bacteriorhodopsin application in optoelectronics. In *Molecular Electronics: Biosensors and Biocomputers*; Hong, F. T., Ed.; Plenum Press: New York, 1989; pp 381–384.
- (24) Hampp, N.; Bräuchle, C.; Oesterhelt, D. *Biophys. J.* **1990**, *58*, 83–93.
- (25) Miyasaka, T.; Koyama, K.; Itoh, I. *Science* **1992**, *255*, 342–344.
- (26) Takei, H.; Lewis, A.; Chen, Z.; Nebenzahl, I. *Appl. Opt.* **1992**, *30*, 500–509.
- (27) Chen, Z.; Birge, R. R. *Trends Biotechnol.* **1993**, *11*, 292–300.
- (28) Rayfield, G. Ultrahigh-speed bacteriorhodopsin photodetectors. In *Molecular Electronics*; Hong, F. T., Ed.; Plenum: New York, 1989; pp 361–368.
- (29) Rayfield, G. Photodiodes based on bacteriorhodopsin. In *Molecular and Biomolecular Electronics*; Birge, R. R., Ed.; Advances in Chemistry Series 240; American Chemical Society: Washington, DC, 1994; pp 561–575.
- (30) Birge, R. R.; Fleitz, P. A.; Gross, R. B.; Izgi, J. C.; Lawrence, A. F.; Stuart, J. A.; Tallent, J. R. *Proc. IEEE EMBS* **1990**, *12*, 1788–1789.
- (31) Song, Q. W.; Zhang, C.; Gross, R.; Birge, R. R. *Opt. Lett.* **1993**, *18*, 775–777.
- (32) Birge, R. R. *IEEE Comput.* **1992**, *25*, 56–67.
- (33) Thoma, R.; Hampp, N. *Opt. Lett.* **1992**, *17*, 1158–1160.
- (34) Thoma, R.; Hampp, N.; Bräuchle, C.; Oesterhelt, D. *Opt. Lett.* **1991**, *16*, 651–653.
- (35) Renner, T.; Hampp, N. *Opt. Commun.* **1992**, *96*, 142–149.
- (36) Hampp, N.; Thoma, R.; Zeisel, D.; Bräuchle, C. *Adv. Chem.* **1994**, *240*, 511–526.
- (37) Zhang, Y. H.; Song, Q. W.; Tseronis, C.; Birge, R. R. *Opt. Lett.* **1995**, *20*, 2429–2431.
- (38) Gu, L. Q.; Zhang, C. P.; Niu, A. F.; Li, J.; Zhang, G. Y.; Wang, Y. M.; Tong, M. R.; Pan, J. L.; Song, Q. W.; Parson, B.; Birge, R. R. *Opt. Commun.* **1996**, *131*, 25–30.
- (39) Lewis, A.; Albeck, Y.; Lange, Z.; Benchowski, J.; Weizman, G. *Science* **1997**, *275*, 1462–1464.
- (40) Birge, R. R.; Govender, D. S. K.; Gross, R. B.; Lawrence, A. F.; Stuart, J. A.; Tallent, J. R.; Tan, E.; Vought, B. W. *IEEE IEDM Technical Digest* **1994**, *94*, 3–6.
- (41) *Molecular electronics and hybrid computers*; Vought, B. W.; Birge, R. R., Eds.; Wiley-Interscience: New York, 1999; Vol. 13, pp 477–490.
- (42) Stuart, J. A.; Tallent, J. R.; Tan, E. H. L.; Birge, R. R. *Proc. IEEE Nonvol. Mem. Technol. (INVMTC)* **1996**, *6*, 45–51.
- (43) Lawrence, A. F.; Stuart, J. A.; Singh, D. L.; Birge, R. R. *Proc. SPIE* **1998**, *3468*, 258–268.
- (44) Bräuchle, C.; Hampp, N.; Oesterhelt, D. *Adv. Mater.* **1991**, *3*, 420–428.
- (45) *CRC Handbook of Organic Photochemistry and Photobiology*; Horspool, W. M., Song, P. S., Eds.; CRC Press: New York, 1995; p 1636.
- (46) Fan, M.-G.; Zhao, W. *Fulvide Family Compounds: Synthesis, Photochromism, and Applications*, 1st ed.; Plenum: New York, 1999; Vol. 1.
- (47) Varo, G.; Lanyi, J. K. *Biochemistry* **1991**, *30*, 5008–5015.
- (48) Kusnetzow, A.; Singh, D. L.; Martin, C. H.; Barani, I.; Birge, R. R. *Biophys. J.* **1999**, *78*, 2370–2389.
- (49) De Groot, H. J. M.; Harbison, G. S.; Herzfeld, J.; Griffin, R. G. *Biochemistry* **1989**, *28*, 3346–3353.
- (50) Luecke, H.; Richter, H. T.; Lanyi, J. K. *Science* **1998**, *280*, 1934–1937.
- (51) Nakanishi, K.; Crouch, R. *Isr. J. Chem.* **1995**, *35*, 253–272.
- (52) Asato, A. E.; Li, X. Y.; Mead, D.; Patterson, G. M. L.; Liu, R. S. H. *J. Am. Chem. Soc.* **1990**, *112*, 7398–7399.
- (53) Hampp, N.; Popp, A.; Bräuchle, C.; Oesterhelt, D. *J. Phys. Chem.* **1992**, *96*, 4679–4685.
- (54) Tan, E. H. L.; Govender, D. S. K.; Birge, R. R. *J. Am. Chem. Soc.* **1996**, *118*, 2752–2753.
- (55) Tallent, J. R.; Stuart, J. A.; Song, Q. W.; Schmidt, E. J.; Martin, C. H.; Birge, R. R. *Biophys. J.* **1998**, *75*, 1619–1634.
- (56) Birge, R. R.; Parsons, B.; Song, Q. W.; Tallent, J. R. Protein-based three-dimensional memories and associative processors. In *Molecular Electronics*; Ratner, M. A., Jortner, J., Eds.; Blackwell Science Ltd.: Oxford, U.K., 1997; pp 439–471.
- (57) Druzko, A. B.; Chamorovsky, S. K. *BioSystems* **1995**, *35*, 133–136.
- (58) Nuss, M. C.; Zinth, W.; Kaiser, W.; Kolling, E.; Oesterhelt, D. *Chem. Phys. Lett.* **1985**, *117*, 1–7.
- (59) Mathies, R. A.; Brito Cruz, C. H.; Pollard, W. T.; Shank, C. V. *Science* **1988**, *240*, 777–779.
- (60) Pollard, W. T.; Cruz, C. H. B.; Shank, C. V.; Mathies, R. A. *J. Chem. Phys.* **1989**, *90*, 199–208.
- (61) Hasson, K. C.; Gai, F.; Anfinsen, P. A. *Proc. Natl. Acad. Sci. U.S.A.* **1996**, *93*, 15124–15129.
- (62) Simmeth, R.; Rayfield, G. W. *Biophys. J.* **1990**, *57*, 1099–1101.
- (63) Birge, R. R.; Finsden, L. A.; Pierce, B. M. *J. Am. Chem. Soc.* **1987**, *109*, 5041–5043.
- (64) Du, M.; Fleming, G. R. *Biophys. Chem.* **1993**, *48*, 101–111.
- (65) Balashov, S. P.; Imasheva, E. S.; Govindjee, R.; Ebrey, T. G. *Biophys. J.*, in press.
- (66) Logunov, S. L.; El-Sayed, M. A. *J. Phys. Chem. B* **1997**, *101*, 6629–6633.
- (67) Tittor, J.; Oesterhelt, D. *FEBS Lett.* **1990**, *263*, 269–273.
- (68) Govindjee, R.; Balashov, S. P.; Ebrey, T. G. *Biophys. J.* **1990**, *58*, 597–608.
- (69) Zeisel, D.; Hampp, N. *J. Phys. Chem.* **1992**, *96*, 7788–7792.

- (70) Thorgeirsson, T. E.; Midler, S. J.; Miercke, L. J. W.; Betlach, M. C.; Shand, R. F.; Stroud, R. M.; Kliger, D. S. *Biochemistry* **1991**, *30*, 9133–9142.
- (71) Drachev, L. A.; Kaulen, A. D.; Khorana, H. G.; Mogi, T.; Otto, H.; Skulachev, V. P.; Heyn, M. P.; Holz, M. *Biochemistry-USSR* **1990**, *54*, 1195–1203.
- (72) Cao, Y.; Váró, G.; Klinger, A. L.; Czajkowsky, D. M.; Braiman, M. S.; Needleman, R.; Lanyi, J. K. *Biochemistry* **1993**, *32*, 1981–1990.
- (73) Yoshida, M.; Ohno, K.; Takeuchi, Y. *J. Biochem.* **1980**, *87*, 491–495.
- (74) Beischel, C. J.; Mani, V.; Govindjee, R.; Ebrey, T. G.; Knapp, D. R.; Crouch, R. K. *Photochem. Photobiol.* **1991**, *54*, 977–983.
- (75) Popp, A.; Wolperdinger, M.; Hampp, N.; Bräuchle, C.; Oesterheld, D. *Biophys. J.* **1993**, *65*, 1449–1459.
- (76) Fischer, U. C.; Towner, P.; Oesterheld, D. *Photochem. Photobiol.* **1981**, *33*, 529–537.
- (77) Tallent, J.; Song, Q. W.; Li, Z.; Stuart, J.; Birge, R. R. *Opt. Lett.* **1996**, *21*, 1339–1341.
- (78) Turner, G.; Miercke, L.; Thorgeirsson, T.; Kliger, D.; Betlach, M.; Stroud, R. *Biochemistry* **1993**, *32*, 1332–1337.
- (79) Tittor, J.; Schweiger, U.; Oesterheld, D.; Bamberg, E. *Biophys. J.* **1994**, *67*, 1682–1690.
- (80) Liu, S. Y.; Ebrey, T. G. *Photochem. Photobiol.* **1987**, *46*, 263–267.
- (81) Birge, R. R.; Zhang, C. F. *J. Chem. Phys.* **1990**, *92*, 7178–7195.
- (82) Birge, R. R.; Gross, R. B.; Masthay, M. B.; Stuart, J. A.; Tallent, J. R.; Zhang, C. F. *Mol. Cryst. Liq. Cryst. Sci. Technol. Sect. B: Nonlinear Opt.* **1992**, *3*, 133–147.
- (83) Huang, J. Y.; Chen, Z.; Lewis, A. J. *Phys. Chem.* **1989**, *93*, 3314–3320.
- (84) Yamazaki, M.; Goodisman, J.; Birge, R. R. *J. Chem. Phys.* **1998**, *108*, 5876–5887.
- (85) Oesterheld, D.; Stoeckenius, W. *Methods Enzymol.* **1974**, *31*, 667–678.
- (86) Becher, B. M.; Cassim, J. Y. *Prepr. Biochem.* **1975**, *5*, 161–178.
- (87) Lorber, B.; DeLucas, L. J. *FEBS Lett.* **1990**, *261*, 14–18.
- (88) Stuart, J. A.; Vought, B. W.; Schmidt, E. J.; Gross, R. B.; Tallent, J. R.; Dewey, T. G.; Birge, R. R. *IEEE EMBS*, in press.
- (89) Shen, Y.; Safinya, C. R.; Liang, K. S.; Ruppert, A. F.; Rothschild, K. J. *Nature* **1993**, *366*, 48–50.
- (90) Lukashov, E. P.; Robertson, B. *Bioelectrochem. Bioenerg.* **1995**, *37*, 157–160.
- (91) Ni, B.; Chang, M.; Duschl, A.; Lanyi, J.; Needleman, R. *GENE* **1990**, *90*, 169–172.
- (92) Cline, S. W.; Doolittle, W. F. *J. Bacteriol.* **1987**, *169*, 1341–1344.
- (93) Ferrando, E.; Schweiger, U.; Oesterheld, D. *Gene* **1993**, *125*, 41–47.
- (94) Parikh, A.; Guengerich, F. *Biotechniques* **1998**, *24*, 428–431.
- (95) Greener, A.; Callahan, M.; Jerpseth, B. *Methods Mol. Biol.* **1996**, *57*, 375–385.
- (96) Greener, A.; Callahan, M.; Jerpseth, B. *Mol. Biotechnol.* **1997**, *7*, 189–195.
- (97) Abdulaev, N. G.; Nabiev, I. R.; Efremov, R. G.; Chumanov, G. *Biol. Membr.* **1986**, *3*, 26–32.
- (98) Thompson, L. K.; McDermott, A. E.; Raap, J.; van der Wielen, C. M.; Lugtenburg, J.; Herzfeld, J.; Griffin, R. G. *Biochemistry* **1992**, *31*, 7931–7938.
- (99) Váró, G.; Duschl, A.; Lanyi, J. K. *Biochemistry* **1990**, *29*, 3798–3804.
- (100) Chizov, I.; Englehard, M.; Chernavskii, D. S.; Zubov, B.; Hess, B. *Biophys. J.* **1992**, *61*, 1001–1006.
- (101) Chang, C. H.; Chen, J. G.; Govindjee, R.; Ebrey, T. *Proc. Natl. Acad. Sci. U.S.A.* **1985**, *82*, 396–400.
- (102) Paek, E. G.; Jung, E. C. *Opt. Lett.* **1991**, *16*, 1034–1036.
- (103) Paek, E. G.; Psaltis, D. *Opt. Eng.* **1987**, *26*, 428–433.
- (104) Gross, R. B.; Izgi, K. C.; Birge, R. R. *Proc. SPIE* **1992**, *1662*, 186–196.
- (105) Parthenopoulos, D. A.; Rentzepis, P. M. *Science* **1989**, *245*, 843–845.
- (106) Marhic, M. E. *Opt. Lett.* **1991**, *16*, 1272–1273.
- (107) Dvornikov, A. S.; Rentzepis, P. M. *Adv. Chem.* **1994**, *240*, 161–178.
- (108) Birge, R. R. *Am. Sci.* **1994**, *82*, 349–355.
- (109) Birge, R. R. *Sci. Am.* **1995**, *272*, 90–95.
- (110) Hunter, S.; Kiamilev, F.; Esener, S.; Parthenopoulos, D. A.; Rentzepis, P. M. *Appl. Opt.* **1990**, *29*, 2058–2066.
- (111) Heanue, J. F.; Bashaw, M. C.; Hesselink, L. *Science* **1994**, *265*, 749–752.
- (112) Curtis, K.; Psaltis, D. *Appl. Opt.* **1992**, *31*, 7425–7428.
- (113) Maeda, A.; Sasaki, J.; Yamazaki, Y.; Needleman, R.; Lanyi, J. K. *Biochemistry* **1994**, *33*, 1713–1717.
- (114) Yamazaki, Y.; Sasaki, J.; Hatanaka, M.; Kandori, H.; Maeda, A.; Needleman, R.; Shinada, T.; Yoshihara, K.; Brown, L.; Lanyi, J. *Biochemistry* **1995**, *34*, 577–582.
- (115) Varo, G.; Lanyi, J. K. *Biochemistry* **1991**, *30*, 5016–5022.
- (116) Lanyi, J.; Varo, G. *Isr. J. Chem.* **1995**, *35*, 365–385.
- (117) Bressler, S.; Friedman, N.; Li, Q.; Ottolenghi, M.; Saha, C.; Sheves, M. *Biochemistry* **1999**, *38*, 2018–2025.
- (118) Fu, X.; Bressler, S.; Ottolenghi, M.; Eliash, T.; Friedman, N.; Sheves, M. *FEBS Lett.* **1997**, *416*, 167–170.
- (119) Govindjee, R.; Misra, S.; Balashov, S. P.; Ebrey, T. G.; Crouch, R. K.; Menick, D. R. *Biophys. J.* **1996**, *71*, 1011–1023.
- (120) Delaney, J.; Scheiger, U.; Subramaniam, S. *PNAS* **1995**, *92*, 11120–11124.
- (121) Greenhalgh, D.; Farrens, D.; Subramaniam, S.; Khorana, H. J. *Biol. Chem.* **1993**, *268*, 20305–20311.
- (122) Subramaniam, S.; Greenhalgh, D.; Rath, P.; Rothschild, K.; Khorana, H. *Proc. Natl. Acad. Sci. U.S.A.* **1991**, *88*, 6873–6877.
- (123) Kandori, H.; Yamazaki, Y.; Hatanaka, M.; Needleman, R.; Brown, L. S.; Richter, H.-T.; Lanyi, J. K.; Maeda, A. *Biochemistry* **1997**, *36*, 5134–5141.
- (124) Balashov, S.; Imasheva, E.; Ebrey, T.; Chen, N.; Menick, D.; Crouch, R. *Biochemistry* **1997**, *36*, 8671–8676.
- (125) Renthall, R.; Chung, Y.; Escamilla, R.; Brown, L.; Lanyi, J. *Biophys. J.* **1997**, *73*, 2711–2717.
- (126) Misra, S.; Ebrey, T.; Crouch, R.; Menick, D. *Photochem. Photobiol.* **1997**, *65*, 1039–1044.
- (127) Miercke, L. J. W.; Betlach, M. C.; Mitra, A. K.; Shand, R. F.; Fong, S. K.; Stroud, R. M. *Biochemistry* **1991**, *30*, 3088–3098.
- (128) Downie, J. D.; Smithy, D. T. *Opt. Lett.* **1996**, *21*, 680–682.
- (129) Dioumaev, A. K.; Brown, L. S.; Needleman, R.; Lanyi, J. K. *Biochemistry* **1999**, *38*, 10070–10078.
- (130) Misra, S.; Govindjee, R.; Ebrey, T. G.; Chen, N.; Ma, J.-X.; Crouch, R. K. *Biochemistry* **1997**, *36*, 4875–4883.
- (131) Zscherp, C.; Heberle, J. *J. Phys. Chem. B* **1997**, *101*, 10542–10547.
- (132) Ahl, P. L.; Stern, L. J.; Mogi, T.; Khorana, H. G.; Rothschild, K. J. *Biochemistry* **1989**, *28*, 10028–10034.
- (133) Dioumaev, A. K.; Richter, H.-T.; Brown, L. S.; Michikazu, T.; Tuzi, S.; Saito, H.; Kimura, Y.; Needleman, R.; Lanyi, J. K. *Biochemistry* **1998**, *37*, 2496–2506.
- (134) Ahl, P. L.; Stern, L. J.; Deuring, D.; Mogi, T.; Khorana, H. G.; Rothschild, K. J. *J. Biol. Chem.* **1988**, *263*, 13594–13601.
- (135) Birge, R. R.; Lawrence, A. F.; Tallent, J. A. *Nanotechnology* **1991**, *2*, 73–87.